SIAM J. APPL. MATH.
Vol. 49, No. 3, pp. 749-783, June 1989

MATHEMATICAL STRUCTURE OF THE BLACK-OIL MODEL FOR PETROLEUM RESERVOIR SIMULATION*

JOHN A. TRANGENSTEIN† AND JOHN B. BELL†

Abstract. This paper describes the three-component black-oil model for petroleum reservoir simulation. This model incorporates compressibility and general mass transfer between phases. It consists of the conditions of thermodynamic equilibrium, an equation of state for the volume balance between the fluid and the rock void, Darcy's Law for the volumetric flow rates, and component conservation equations. These relations are manipulated to form a pressure equation and a modified system of component conservation equations. It is shown that the pressure equation is parabolic and that, in the absence of diffusive forces such as capillary pressure and mixing, the component conservation equations are hyperbolic, subject to technical conditions on the relative permeabilities. This sequential formulation of the flow equations forms the basis for a numerical solution method for the system. This numerical method is used to illustrate the types of wave structures that occur for the system.

Key words. hyperbolic conservation law, Godunov's method, reservoir simulation, shock

1. Introduction.

1.1. Overview of sequential methods for reservoir simulation. The black-oil fluid model is the standard phase behavior model most often used in petroleum reservoir simulation. It is able to predict compressibility and mass transfer effects between phases that are needed to model primary (pressure depletion) and secondary (water injection) recovery. The importance of the black-oil model for reservoir engineering studies makes it an important model for study by researchers interested in developing new methods for solution of the equations of multiphase flow in porous media.

In this paper we analyze the mathematical structure of the black-oil flow equations. Reservoir fluid flow exhibits behavior typical of the solutions of both parabolic and hyperbolic partial differential equations. For example, pressure effects are quickly felt throughout the reservoir. On the other hand, injected materials flow with a finite speed of propagation, and solutions often develop sharp fronts separating different fluid states. (For more discussion of this behavior as well as numerical examples, see [3].) Our principal motivation for decoupling the equations is the development of a sequential numerical algorithm. By decoupling the equations into their parabolic and hyperbolic components, we can develop numerical methods appropriate to each type of behavior.

The black-oil flow equations consist of the conditions of thermodynamic equilibrium (which determines how the components combine to form phases), an equation of state (which states that the fluid fills the pore volume), Darcy's Law for the volumetric flow rates, and a mass conservation equation for each component. Inherently, sequential methods cannot satisfy all of the flow equations exactly at each step of the computation; some incompatibility must be introduced. We satisfy thermodynamic equilibrium, Darcy's Law, and the component conservation equations exactly, but we linearize the equation of state so that it is only satisfied approximately.

Several authors have proposed "volume-discrepancy" splittings, so-called because of their linearization of the volume balance equation. Acs, Doleschall, and Farkas [1] have developed a pressure equation similar to the pressure equation discussed later

* Received by the editors January 27, 1987; accepted for publication (in revised form) May 5, 1988.
† Exxon Production Research Company, P.O. Box 2189, Houston, Texas 77252-2189. Present address, Lawrence Livermore National Laboratory, P.O. Box 808, Livermore, California 94550.

in this paper; however, the conservation of mass equations were treated directly in a discretized form similar to early IMPES methods. This approach, which decoupled the equations at a discrete level, did not correctly separate the hyperbolic part of the system from the parabolic part of the system at a differential equation level. Watts [13] and Kendall et al. [9] have described an alternative volume discrepancy splitting in which the pressure equation was used to obtain a total fluid velocity. However, these authors proposed a further decomposition of the system into saturation equations and molar (component conservation) equations.

The sequential approach discussed in this paper combines elements of each of these methods. Our pressure equation is derived from a total volume balance similar to the approach discussed by Watts [13]. We write component conservation equations based on a total velocity splitting rather than the IMPES type approach of Acs, Doleschall, and Farkas [1]. However, the component conservation equations are treated with saturations determined as functions of composition as in [1] rather than a further decomposition into saturation equations and molar equations as in [13].

We note that a mass-conserving sequential method that also avoids a volume discrepancy error has been constructed (see [3]). In that method a linearized equation of state was used to develop a pressure equation as in the above methods, but this equation was used only to provide a total fluid velocity for the conservation equations. The pressure used in the component conservation equation was determined implicitly by the equation of state. From an analytical point of view this approach is perhaps the most satisfying; however, it introduces considerable computational complexity. In particular, the implicit dependence of pressure on composition greatly complicates the accurate prediction of the flux for the component conservation equations by coupling the nonlinear equation of state to the conservation law. The volume discrepancy approach of this paper avoids this complication.

1.2. Black-oil flow equations. Before we discuss the details of the black-oil thermodynamic model, let us describe the flow equations in very general terms. We consider the reservoir fluid to be made of three components: oil, gas, and water. The mass per unit pore volume of each of these components in the total fluid is denoted by the vector n. To reach thermodynamic equilibrium, these components combine to form at most three phases: liquid, vapor, and aqua. Given n and the pressure p, the black-oil model describes thermodynamic equilibrium by determining the matrix N of masses of each component in each phase per pore volume. This is done in such way that the fluid mass is balanced among the phases; i.e.,

$$n = Ne. \tag{1.1}$$

(Here, e is a vector of ones.) In addition, the black-oil model uses n and p to compute the vector u of ratios of the phase volumes to the pore volume. From this, we derive the equation of state

$$e^T u = 1, \tag{1.2}$$

which states that the sum of the phase volumes is equal to the pore volume.

The flow of the reservoir fluid is specified in terms of volumetric flow rates v_p for each of the phases. These are given by Darcy's Law:

$$v_p = -\lambda_p \left(\frac{\partial p}{\partial x} - \rho_p \frac{\partial d}{\partial x} \right) \kappa, \tag{1.3}$$

where λ_p is the phase mobility, ρ_p is the phase density, κ is the rock permeability, and d is depth as a function of the coordinate x.

Finally, we require that the mass of each component is conserved. If we let D_u be a diagonal matrix formed from the entries of u, then ND_u^{-1} represents the density of each component in each phase. Thus, we have the conservation of mass equation

$$\frac{\partial(n\phi)}{\partial t}+\frac{\partial}{\partial x}(ND_u^{-1}\mathrm{v})=0, \tag{1.4}$$

where ϕ is porosity and v is the vector of phase velocities. If we use the auxiliary relations (1.1) and (1.3) to reduce the system, we obtain a system of conservation equations (1.4) for the component densities n in terms of the pressure p and the component densities, and an equation of state (1.2). A more complete description and detailed discussion of the functional dependence of all the variables will appear in the text below.

1.3. Outline. The system of equations (1.1)–(1.4) describes multiphase flow in porous media in very general terms. As can be seen from the above discussion, the thermodynamic model plays a crucial role in specifying a particular flow model. In § 2 we describe the black-oil thermodynamic model in its most general form. There we discuss mass transfer, undersaturation, and compressibility and describe the equation of state. In § 3 we discuss Darcy's Law and examine the models used for viscosity, relative permeability, and mass density. In § 4, we introduce a splitting of the governing equations that forms the basis for the sequential method. First, we derive a pressure equation by linearizing the equation of state. The pressure gradient is also used to compute a total fluid velocity. Then we derive a system of component conservation equations based on rewriting the conservation equations (1.4) in terms of the total velocity. In § 5, we analyze the pressure equation and show that it is parabolic, provided that the parameters appearing in the black-oil fluid model have been properly specified. In § 6, we perform a characteristic analysis of the component conservation equations, showing that they form a hyperbolic system under certain technical but nonrestrictive assumptions. In § 7, we briefly discuss a numerical method for solving the flow equations in which the component conservation equations are discretized using a second-order Godunov method. The numerical method is used to illustrate the types of wave structures characteristic of the full system of equations. The paper also contains two appendices. In Appendix A, we present the units we have used for reservoir simulation and we provide explicit functional forms for several black-oil models. In Appendix B, we give the characteristic structure for an alternative form of the component conservation equations.

Before discussing the black-oil model in greater detail, we first examine the scope of the analysis considered here. The thermodynamic model is the most general form possible within the black-oil framework. Although not discussed in detail, we also allow for essentially arbitrary spatial variation in the parameters describing the reservoir, namely, porosity and permeability. Finally, the development of the flow equations and their analysis in the following sections are given in one dimension only; however, the extension to multiple dimensions involves little more than a change of notation. In particular, the pressure equation remains parabolic and the component conservation equations remain hyperbolic in multiple dimensions.

The work described in this paper does not include the effects of capillary pressure and dispersive mixing. The effect of these terms is to introduce extremely complicated dissipative terms into the component conservation equations. For most problems in reservoir simulation, these terms are quite small relative to the length scale of the simulation and can be ignored. When they are included, the component conservation

equations become transport-dominated parabolic equations. From the algorithmic point of view, inclusion of additional dissipative terms presents no serious problems; the difficulties lie in computing meaningful weak solutions in the absence of regularizing diffusive terms.

2. The black-oil thermodynamic model and equation of state. In this section we describe the black-oil thermodynamic model in detail. This model provides the fluid description that is used to determine the equilibrium distribution (1.1) of the components among the phases. This same model of fluid behavior is also used to evaluate the equation of state (1.2). In addition, it provides information needed to compute the Darcy velocities (1.3) and the flux in the component conservation equations (1.4).

In § 2.1 we discuss the meanings of "components" and "phases." We examine the interplay between these two quantities due to mass transfer. In § 2.2, we show how to determine the number of phases actually formed, and how to solve the phase equilibrium problem when all phases are formed. In § 2.3 we solve the phase equilibrium problem when one of the phases is missing due to undersaturation. Finally, we discuss compressibility and formulate the equation of state in § 2.4.

2.1. Components and phases. As we mentioned in the Introduction, we consider the reservoir fluid to be made of three components: oil, gas, and water. In practice, these are the separations that the reservoir fluid naturally chooses at surface temperature and pressure. Within the reservoir, the components mix with one another to form at most three phases: liquid, vapor, and aqua. It is convenient to distinguish components from phases by the following mnemonic: components may be thought to correspond to chemical molecules, whereas phases are homogeneous mixtures of these molecules separated from other phases by a fluid interface.

The black-oil model can include a variety of thermodynamic effects. The description of three-component black-oil with gas dissolved in the liquid phase is fairly standard; see, for example, [2], [11]. Other authors [12] have described black-oil models that allow oil to volatilize into the vapor phase. In this section we describe a general black-oil model, with dissolved gas in two phases as well as volatile oil. The previously cited models are special cases of the model presented below.

Because the components flow in phases but are conserved by mass, it is necessary to understand how the mass of each component in the fluid is apportioned into phases. We assume that at each point of the reservoir the components associate into phases in order to attain thermodynamic equilibrium. In the context of the black-oil model, this means that we want to solve the following *phase equilibrium problem*: given the pressure p and the vector

$$n = \begin{bmatrix} n_o \\ n_g \\ n_w \end{bmatrix}$$

of the component densities in the total fluid, find the matrix

$$N \equiv \begin{bmatrix} n_{ol} & n_{ov} & 0 \\ n_{gl} & n_{gv} & n_{ga} \\ 0 & 0 & n_{wa} \end{bmatrix}$$

of component densities in each of the phases, subject to the mass-balance condition (1.1), which is $n = Ne$. Of course, we have not yet provided enough information to determine N from n and p. This information will be provided in §§ 2.2–2.3 below.

The dimensions of n and N are mass per *pore* volume. Note that the definition of N indicates the maximum extent to which the components are allowed to mix in the reservoir phases. Oil may be allowed to appear in the liquid and vapor phases, gas may be allowed in all three phases, and water is permitted in the aqueous phase only. Oil and water do not mix, and water vapor (steam) is not treated.

2.2. Mass transfer and phase equilibrium. In the previous section, we have qualitatively discussed the possible compositions of the various phases. In this section we provide a quantitative description of mass transfer to determine which phases are formed, and how much of each component appears in each phase.

In the black-oil model we associate to each phase a principal component. In particular, we associate oil with the liquid phase, gas with the vapor phase, and water with the aqueous phase. The amount of each component in each phase in related to the amount of the principal component in that phase by a ratio matrix R. When all three phases are formed, R is a known function of pressure that satisfies

$$\begin{bmatrix} 1 & R_v & 0 \\ R_l & 1 & R_a \\ 0 & 0 & 1 \end{bmatrix} \equiv R = ND_N^{-1}. \tag{2.1}$$

Here D_N is the diagonal part of N, which represents the principal component densities in each phase. Note that R is dimensionless.

Of course, the functions defining R are not completely arbitrary. The ratios R_l, R_v, and R_a must be nonnegative functions. We also require that if either of the ratios R_l or R_a is positive anywhere, its derivative is strictly positive for all pressures. (The reason for these requirements are discussed in § 2.3.1.) Further, we require that $\det R > 0$ so that the phase volumes are nonnegative (see (2.18) below), so that the matrix R is nonsingular, and so that the undersaturation cases are mutually exclusive (see § 2.3). Note that it is not necessary for the derivative of R_v to be positive when R_v is nonzero. Also note that it is not necessary for all of the ratios to be strictly positive; in fact, the standard dissolved-gas black-oil model takes both of the ratios R_v and R_a to be identically zero.

At this point, we have all the information that is needed to determine how many phases will be formed. Furthermore, if all three phases are formed we can solve the phase equilibrium problem. Given the pressure p we compute the ratio matrix R with the ratios evaluated at the given pressure and define

$$T \equiv R^{-1}.$$

We then form the vector Tn. If all three entries of the vector Tn are positive, then all three phases are formed. In this case, we say that the fluid is *saturated*, and we can show, using (1.1) and (2.1), that D_N is given by

$$D_N e = Tn. \tag{2.2}$$

Furthermore, when the fluid is saturated, the solution to the phase equilibrium problem is computed by

$$N = RD_N. \tag{2.3}$$

Equations (2.2)–(2.3) provide a complete description of the solution of the phase equilibrium problem when all three phases are formed. We now turn our attention to the remaining cases in which some of the phases are not formed.

2.3. Undersaturation. Although the black-oil model involves three components, this does not necessarily mean that three phases are always formed. For example, if gas is allowed to dissolve in liquid, then for sufficiently high pressures it is possible for all the gas to dissolve in the liquid phase, and for the vapor phase to disappear. In such a case, the liquid is said to be *undersaturated.* When oil is allowed to volatilize into vapor, it is also possible that for extreme pressures no liquid will be formed and the vapor phase will be undersaturated. We remark that we have at most two cases to consider: all gas dissolved in liquid and/or aqua, or all oil dissolved into vapor. There are no other cases of undersaturation, because water is not allowed to appear in either liquid or vapor.

The entries of Tn provide the key to which phases are present. A phase is present if and only if the corresponding element of Tn is positive. Before discussing the phase equilibrium problems, we show that at most one element of Tn is negative; i.e., at most one phase can be missing due to undersaturation.

First we consider the case in which the liquid and aqueous phases are undersaturated and the vapor phase is missing. When this occurs the vapor component of Tn is negative; that is,

$$e_v^T Tn = \frac{n_g - R_l n_o - R_a n_w}{1 - R_l R_v} < 0.$$

(Here e_v is the vector with one in the vapor phase entry and zeroes elsewhere.) By solving this inequality for $n_g/(1 - R_l R_v)$, it is easy to see that this inequality implies that the liquid component of Tn is nonnegative:

$$e_l^T Tn = \frac{n_o - R_v n_g + R_v R_a n_w}{1 - R_l R_v} \geqq n_0 \geqq 0.$$

Thus if the vapor phase is missing and any oil is present, then a liquid phase must be formed.

Similarly, when oil is volatile and the vapor phase is undersaturated, the liquid component of Tn in (2.2) is negative; that is,

$$e_l^T Tn = \frac{n_o - R_v n_g + R_v R_a n_w}{1 - R_l R_v} < 0.$$

Since we have assumed that $\det R = 1 - R_l R_v > 0$, it is easy to see that $R_v > 0$ and that the amount of gas in vapor is positive:

$$n_g - R_a n_w > \frac{n_0}{R_v} \geqq 0.$$

By solving the expression for the liquid component of Tn in terms of n_o, it is easy to see that the vapor component of Tn is nonnegative:

$$e_v^T Tn = \frac{n_g - R_l n_o - R_a n_w}{1 - R_l R_v} > n_g - R_a n_w > 0.$$

Thus if the liquid phase is missing and any gas is present, then a vapor phase must be formed.

2.3.1. Vapor phase missing. We now examine the first undersaturation case in more detail. The physical meaning of the negative vapor component of Tn is that the fluid pressure p is higher than the *bubble-point pressure* p_b, at which vapor phase forms.

This bubble-point pressure is implicitly defined by the requirement that the vapor component of D_N be zero:

$$0 = -R_l(p_b)n_o + n_g - R_a(p_b)n_w. \tag{2.4}$$

Note that the requirement that R_l and R_a be increasing when they are nonzero means that there is at most one bubble-point pressure p_b. Also note that this same requirement implies $p_b < p$. Finally, the functions R_l and R_a must be defined for the entire expected range of reservoir pressures *and* bubble point pressures so that (2.4) can be solved.

At this point it is easy to solve the phase equilibrium problem when the vapor phase is missing. First, we compute the bubble-point pressure p_b using (2.4). Next, we evaluate the ratios $\bar{R}_l$ and $\bar{R}_a$ at p_b. (Here, the bars are used to distinguish the ratios evaluated at p_b from those evaluated at p.) Since there is no vapor phase, all of the oil must be in liquid and all of the water must be in aqua; in other words,

$$D_N = \text{diag}\,(n_o, 0, n_w). \tag{2.5}$$

As a result, the definition (2.1) of R shows that

$$N = RD_N = \begin{bmatrix} n_o & 0 & 0 \\ \bar{R}_l n_o & 0 & \bar{R}_a n_w \\ 0 & 0 & n_w \end{bmatrix}. \tag{2.6}$$

Note that the volatile oil ratio R_v does not appear in the solution of the phase equilibrium problem when the vapor phase is missing.

2.3.2. Liquid phase missing. Now we examine the other case of undersaturation in more detail. If the liquid phase is missing, we need a new variable to take the role of the bubble-point pressure in the previous section. Accordingly, we define the volatile oil ratio in order to make the liquid component of Tn be zero:

$$\bar{R}_v = \frac{n_o}{n_g - R_a(p)n_w}. \tag{2.7}$$

Note that the volatile oil ratio $\bar{R}_v$ defined by (2.7) must be less than $R_v(p)$ used in (2.3).

A reader who is unfamiliar with the black-oil model might try to define a *dew point pressure* to describe the point at which the liquid phase is emergent. However, such a pressure would not be uniquely defined, since reservoir fluids with volatile oil often have two dew point pressures. (This is reflected in the fact, mentioned in § 2.2, that R_v is not necessarily a monotone function of pressure.) Consequently, we will work with the volatile oil ratio $\bar{R}_v$ directly.

At this point, it is easy to solve the phase equilibrium problem with an undersaturated vapor phase. First, we compute $\bar{R}_v$ using (2.7). There, the ratio R_a remains the same function of p as in the saturated case. Since there is no liquid phase, the amount of gas in vapor must equal the total amount of gas in the fluid minus the amount of gas dissolved in aqua, and all of the water must be in aqua; in other words,

$$D_N = \text{diag}\,(0, n_g - R_a n_w, n_w). \tag{2.8}$$

Then the definition (2.1) of R implies that

$$N = RD_N = \begin{bmatrix} 0 & \bar{R}_v(n_g - R_a n_w) & 0 \\ 0 & n_g - R_a n_w & R_a n_w \\ 0 & 0 & n_w \end{bmatrix}. \tag{2.9}$$

2.3.3. Combined formulation of undersaturated phase behavior. In this section we introduce some special notation that allows us to unify the description of the undersaturated phase equilibrium problem. This unified description will eliminate the need for treating each undersaturation case separately in the remainder of the text and will help clarify the relationship between the saturated and undersaturated characteristic analysis in § 6. The basic idea will be to reexpress the relationships described in §§ 2.3.1 and 2.3.2 in a reduced matrix-vector form that parallels the structure of the saturated equations.

For the case when the vapor phase is missing, we define

$$Q \equiv \begin{bmatrix} 1 & 0 \\ 0 & 0 \\ 0 & 1 \end{bmatrix}, \quad q \equiv \begin{bmatrix} 0 \\ 1 \\ 0 \end{bmatrix}, \quad \omega \equiv p_b.$$

When the liquid phase is missing, we define

$$Q \equiv \begin{bmatrix} 0 & 0 \\ 1 & 0 \\ 0 & 1 \end{bmatrix}, \quad q \equiv \begin{bmatrix} 1 \\ 0 \\ 0 \end{bmatrix}, \quad \omega \equiv \bar{R}_v.$$

If we now define

$$\bar{t} \equiv \begin{bmatrix} -R_l(p_b) \\ 1 \\ -R_a(p_b) \end{bmatrix} \tag{2.10a}$$

when the vapor phase is missing, or

$$\bar{t} \equiv \begin{bmatrix} 1 \\ -\bar{R}_v \\ 0 \end{bmatrix} \tag{2.10b}$$

when the liquid phase is missing, then the value of the undersaturation parameter, ω, is determined by the equation

$$0 = n^T \bar{t}. \tag{2.11}$$

This equation is equivalent to (2.4) or (2.7).

Next, we define the matrix

$$\bar{R} \equiv RQ, \tag{2.12}$$

which has the column corresponding to the missing phase deleted. We also define a left inverse for $\bar{R}$ given by

$$\bar{T} \equiv \begin{bmatrix} 1 & 0 & 0 \\ 0 & 0 & 1 \end{bmatrix}$$

if the vapor phase is missing, and

$$\bar{T} \equiv \begin{bmatrix} 0 & 1 & -R_a \\ 0 & 0 & 1 \end{bmatrix}$$

if the liquid phase is missing. Note that $\bar{T}$ depends on p when the liquid phase is missing; however, in neither case does it depend on ω. On the other hand, $\bar{R}$ depends

on ω in both cases, and depends on p when the liquid phase is missing. Observe that, as noted above, $\bar{T}$ is a left-inverse for $\bar{R}$:

$$\bar{T}\bar{R} = I, \tag{2.13}$$

and that $\bar{t}$ is orthogonal to the columns of $\bar{R}$:

$$\bar{R}^T\bar{t} = 0. \tag{2.14}$$

If we let

$$\bar{D}_N \equiv Q^T D_N Q,$$

then the solution of the phase equilibrium problem is given by

$$\bar{D}_N e = \bar{T} n, \tag{2.15}$$

$$N = \bar{R}\bar{D}_N Q^T. \tag{2.16}$$

Note that equations (2.15)–(2.16) are equivalent to (2.5)–(2.6) when the vapor phase is missing and they are equivalent to (2.8)–(2.9) when the liquid phase is missing. Also note the similarity between the undersaturated formulae (2.15)–(2.16) and the saturated formulae (2.2)–(2.3).

2.4. Compressibility and the equation of state. Even though water and oil have small compressibilities, the high compressibility of gas and the swelling effect caused by gas dissolving in liquid lead to important volume changes at reservoir pressures. The black-oil model incorporates these volume changes by relating the reservoir volumes of each of the phases to the amounts of the principal component in that phase. To quantitatively define this relationship, we let

$$D_u \equiv \text{diag}\,(u_l, u_v, u_a) = \text{diag}\,(u)$$

be the diagonal matrix of phase volumes per pore volume. We distinguish these variables from the phase saturations (see § 3.1), whose units are reservoir phase volume per reservoir fluid volume. This distinction plays an important role in the volume-discrepancy sequential method described in § 4, where we linearize the equation of state (1.2), rather than requiring it to be satisfied exactly.

The entries of D_N and D_u are related by the formation volume factors B. When all three phases are formed, B is a diagonal matrix of known functions of pressure that satisfy

$$\begin{bmatrix} B_l & 0 & 0 \\ 0 & B_v & 0 \\ 0 & 0 & B_a \end{bmatrix} \equiv B = D_u D_N^{-1}. \tag{2.17}$$

The formation volume factors have the dimensions of a specific volume, i.e., phase volume per dominant component mass.

The functions of pressure that define B are not completely arbitrary. Obviously, B must be positive definite. In the absence of mass transfer, an increase in pressure would decrease the volume of each of the phases; in such a case the first derivative of B should be negative. When gas dissolves in liquid, the formation volume factor B_l must change its pressure dependence to reflect the effects of undersaturation. Below the bubble point, an increase in pressure can lead to an *increase* in the liquid phase volume, representing swelling effects caused by gas dissolving into the liquid phase. Above the bubble point, an increase in pressure can only serve to *decrease* the liquid phase volume. Thus, the undersaturated formation volume factor $\bar{B}_l$ must be a function

of both p and p_b when the liquid phase is undersaturated. A similar statement holds for the aqueous phase when gas is allowed to dissolve in it. We also note that the undersaturated vapor formation volume factor $\bar{B}_v$ must be taken to be a function of p and $\bar{R}_v$ when vapor is undersaturated. Finally, we note that there are also certain physical constraints on B that are discussed in detail in § 5.2 when we examine the pressure equation.

We now discuss the computation of the phase volumes. When the fluid is saturated, we use the pressure to compute the matrix B of formation volume factors. Then the vector of phase volume fractions u is given by

$$u = BTn. \tag{2.18}$$

When the fluid is undersaturated, we define the diagonal matrix of modified formation volume factors

$$\bar{B} \equiv Q^T BQ.$$

After computing $\bar{B}$, we compute the phase volumes from

$$u = Q\bar{B}\bar{T}n. \tag{2.19}$$

Note that the vapor formation volume factor B_v and the volatile oil ratio R_v are unnecessary for the determination of the phase volumes with the vapor phase missing. Similarly, B_l and R_l are not needed to compute the phase volumes when the liquid phase is missing. Note the similarity of the undersaturated equation (2.19) to the saturated formula (2.18).

The ultimate purpose of this discussion of the phase volume determination is to describe the equation of state. As we saw in the introduction, the equation of state simply says that the reservoir fluid must fill the pore volume. Since the vector u has units of phase volume per pore volume, we require that the sum of the phase volumes equal the pore volume; i.e., (1.2) holds.

3. Darcy's Law. In the previous section we examined the black-oil thermodynamic model. To complete the description of the flow equations we must specify how the phases flow through the reservoir. For the black-oil model, the phase velocities are typically specified by Darcy's Law.

In one spatial dimension with gravitational effects, the vector of Darcy phase velocities given in (1.3) can be written in matrix-vector form as

$$\mathrm{v} = -L\left(e\frac{\partial p}{\partial x} - \rho\frac{\partial d}{\partial x}\right)\kappa. \tag{3.1}$$

Here,

$$L \equiv \operatorname{diag}\left(\frac{\kappa_l}{\mu_l}, \frac{\kappa_v}{\mu_v}, \frac{\kappa_a}{\mu_a}\right)$$

is the diagonal matrix of phase mobilities (i.e., phase relative permeability divided by phase viscosity),

$$\rho \equiv \begin{bmatrix} \rho_l \\ \rho_v \\ \rho_a \end{bmatrix}$$

is the vector of phase densities, and κ is the total rock permeability. The units of κ are chosen so that the phase velocity vector v has units of phase volume per flow area

per time. Also, d is depth as a function of reservoir location times a gravitational constant. The depth gradient $\partial d/\partial x$ and the total permeability κ are allowed to be functions of the spatial coordinate x. We have ignored capillary pressure, so that the pressure in each phase is p.

To determine the phase velocities we need to specify the phase mobilities L and the phase densities ρ. In the remainder of this section we discuss the functional dependence of relative permeabilities, viscosities, and phase densities. Explicit forms typical of these functions are described in the Appendix A.

3.1. Saturations. Saturations are the fractions of the *fluid* volume occupied by each of the phases. We define the vector of phase saturations by

$$s \equiv u \frac{1}{e^T u}. \tag{3.2}$$

With this definition, the saturations are all nonnegative, and sum to one even if the equation of state (1.2) is not satisfied exactly. Again, we reiterate that the saturations s must be considered to be distinct from the vector u of ratios of phase volumes to pore volume. This distinction plays an important role in the volume-discrepancy sequential method described in the next section.

3.2. Relative permeability. Relative permeabilities describe how the presence of each phase adversely affects the flow of the other phases. For a water-wet rock, the aqueous phase lines the pore cavities, whereas the vapor phase exists in bubbles away from the pore walls. Typically, the liquid phase is more likely to line the pore walls than the vapor phase, but less likely to do so than the aqua phase. In other words, the liquid phase typically has intermediate wettability [7].

The relative permeabilities are properties of the relative sizes of the phases, the rock, the past history of the flow, and the interfacial tension between the phases. Because of the complex interaction of the phases with the pore space, the exact dependence on rock and fluid properties is not fully understood. It is known, however, that as the saturation of a phase goes to zero, its mobility must also tend to zero; this implies that its relative permeability vanishes. Furthermore, it is generally the case that a phase will, in fact, become immobile before its saturation reaches zero.

We assume that the relative permeabilities are nonnegative functions of the phase saturations and the spatial coordinate only. We have defined the saturations so that they sum to one; hence, we can express one of the saturations and all of the relative permeabilities in terms of the other two saturations.

3.3. Viscosity. Viscosity is a property of a phase that represents its resistance to flow under the influence of a pressure gradient. Viscosities are always positive. The viscosity of liquid is generally a decreasing function of pressure when the liquid phase is saturated, due to the influence of the dissolved gas. If gas does not dissolve in liquid, or if the liquid phase is undersaturated, then the liquid viscosity is an increasing function of pressure. Thus when liquid is undersaturated, the liquid viscosity depends on both p and the bubble point pressure p_b. The viscosity of aqua behaves similarly, although its pressure dependence is much smaller. The viscosity of vapor is generally an increasing function of p.

3.4. Phase density. In order to determine the effects of gravity on the flow of the phases through the reservoir, we need to compute the phase densities. In the definition of the mass densities we include a vector w which scales the component densities. This

scaling is required because of the units used in black-oil simulation (see Appendix A). If all the phases are saturated, then

$$\rho = B^{-1} R^T w;$$

whereas, for the undersaturated cases we have

$$Q^T \rho = \bar{B}^{-1} \bar{R}^T w.$$

Note that the mass density of the phase missing due to undersaturation can be given an arbitrary value. This is because the mobility term in Darcy's Law that multiplies the density is zero for a missing phase; i.e., the missing phase has zero phase velocity.

3.5. The phase velocity functional dependence. Before describing the sequential formulation of the equations, we summarize the functional dependencies of the phase velocities. When the fluid is saturated, v is a function of p, s, x, and the pressure gradient. When the fluid is undersaturated, v is a function of p, s, x, the pressure gradient, and the undersaturation variable ω.

4. A sequential formulation of the black-oil equations. In §§ 2 and 3 we discussed the basic equations governing the black-oil thermodynamic model and black-oil fluid flow. Using these equations we can explicitly evaluate the flux appearing in the mass conservation equation (1.4). In particular, for saturated flow the component flux is

$$ND_u^{-1} \mathrm{v} = RB^{-1} \mathrm{v}. \tag{4.1}$$

Similarly, for an undersaturated fluid we have

$$ND_u^{-1} \mathrm{v} \equiv NQD_{Q^T u}^{-1} Q^T \mathrm{v} = \bar{R}\bar{B}^{-1} Q^T \mathrm{v}. \tag{4.2}$$

Here the left-hand side of (4.2) is understood to ignore terms involving zero phase velocity over zero phase volume, as is correctly represented by the middle term. The black-oil model also provides us with the necessary information to evaluate the quantities required for computing the phase velocities in Darcy's Law.

As mentioned in the Introduction, computational results and analogies with model problems indicate that the combined black-oil flow system (1.1)-(1.4) exhibits both parabolic and hyperbolic behavior. In this section we introduce a sequential splitting of the equations into a pressure equation and a system of component conservation equations. In the subsequent sections we show that the pressure equation is parabolic, and that the component conservation equations are hyperbolic.

The basic idea behind the sequential splitting of the equations is that, over some time interval, we first solve for the pressure with the composition fixed and compute a total velocity. Then we solve for the new composition with the pressure and total velocity fixed. Thus, the sequential method is based on alternately freezing some of the unknowns over a specific time interval, which we denote by Δt.

4.1 The pressure equation. The first step in the sequential approach is to develop a differential equation for pressure. This pressure equation represents a total volume balance. In particular, given the pressure p and fluid composition n at the current time level t, we want to predict the value of the pressure at the advanced time level $t + \Delta t$, so that the equation of state (1.2) will be satisfied. If we linearize (1.2) about time t we obtain

$$\frac{1 - e^T u}{\Delta t} = e^T \frac{\partial u}{\partial p} \frac{\partial p}{\partial t} + e^T \frac{\partial u}{\partial n} \frac{\partial n}{\partial t}.$$

Note that we have not assumed that the equation of state (1.2) is satisfied at the current time level; in fact, we want to choose the pressure to correct any existing volume discrepancy errors. Next, we multiply by the porosity ϕ and use the mass conservation equation to replace the time derivative of n:

$$\frac{e^T u - 1}{\Delta t}\phi = \left[-\phi e^T \frac{\partial u}{\partial p} + e^T \frac{\partial u}{\partial n} n \frac{\partial \phi}{\partial p}\right]\frac{\partial p}{\partial t} + e^T \frac{\partial u}{\partial n}\frac{\partial}{\partial x}(ND_u^{-1}\mathrm{v}) \tag{4.3}$$

where the phase velocities are functions of the pressure gradient as given by (3.1). Equation (4.3) establishes the basic form of the pressure equation for the sequential method. In § 5 we show that it is actually a parabolic equation for pressure.

4.2. The component conservation equations. Next we want to derive the system of component conservation equations used in the second step of the sequential method. Here the basic idea is to define a total velocity describing net flow of fluid, and use it to eliminate the pressure gradient term appearing in Darcy's Law. The motivation for this step is that for incompressible model problems a total velocity splitting correctly decouples the elliptic and hyperbolic behavior inherent in the equations.

The total fluid velocity is the sum of the phase velocities; i.e.,

$$\mathrm{v}_T \equiv e^T \mathrm{v} = -e^T Le \frac{\partial p}{\partial x}\kappa + e^T L\rho \frac{\partial d}{\partial x}\kappa.$$

Next, we use the expression for v_T to solve for the pressure gradient, and substitute into expression (3.1). This gives us the following expression for the Darcy velocities:

$$\tilde{\mathrm{v}} = Le\frac{1}{e^T Le}\mathrm{v}_T + \left[I - Le\frac{1}{e^T Le}e^T\right]L\rho\frac{\partial d}{\partial x}\kappa. \tag{4.4}$$

Replacing v by $\tilde{\mathrm{v}}$ in the mass conservation equation (1.4) gives us

$$\frac{\partial n\phi}{\partial t} + \frac{\partial h}{\partial x} = 0 \tag{4.5}$$

where the sequential component flux is

$$h = RB^{-1}\tilde{\mathrm{v}} \tag{4.6}$$

when the fluid is saturated, and

$$h = \bar{R}\bar{B}^{-1}Q^T\tilde{\mathrm{v}} \tag{4.7}$$

when the fluid is undersaturated. Henceforth, we drop the tilde over the phase velocities used in the conservation law; it is understood that the phase velocities in the component conservation equations are expressed in terms of the total velocity. Equation (4.5) with the flux given by (4.6)–(4.7) is the system of component conservation equations for the sequential method. In § 6, we present a characteristic analysis of this system showing that it is hyperbolic under suitable restrictions on the relative permeability model.

This splitting of the equations allows us to conserve mass at the expense of developing a volume discrepancy error. However, splitting the equations in this manner also has another interesting consequence. If the pressure were known in the unsplit form of the equations, the equation of state would allow us to eliminate one of the component densities from the system. (We cannot do this and retain mass conservation because of the volume discrepancy.) Thus in some sense we have an extra equation in (4.5). This extra equation appears in the wave structure as a degenerate linear advection mode that carries essentially no information. In this context, the original

distinction between u and s plays an interesting role. Before splitting, u and s are the same; hence, D_s^{-1} could equally well have been used in formulating (1.4). In the sequential method these quantities are not the same. However, their essential difference is displayed by changing the structure of the "artificial" wave introduced by the splitting. Numerically, it makes little difference which version is used. Because the characteristic analysis in § 6 is intricate, we have chosen to derive the easier case and merely state the differences for the alternative approach.

5. Analysis of the pressure equation. In the previous section we developed the pressure equation (4.3) from a volume balance. In this section we show that it is, in fact, parabolic. The analysis of the pressure equation depends on two properties of the fluid model. First, there are certain homogeneity properties of the phase volumes that allow us to simplify the form of (4.3). Second, there are conditions describing the overall compressibility of the total rock-fluid system that guarantee that the equation is parabolic.

5.1. Partial phase volumes. To form the pressure equation (4.3), we use the partial derivatives of the phase volumes taken with respect to the component vector n, for fixed pressure. If the fluid is saturated, then this matrix of *partial phase volumes* is computed using (2.18):

$$\frac{\partial u}{\partial n} = BT. \tag{5.1}$$

Note that the phase volumes satisfy the homogeneity relationship:

$$\frac{\partial u}{\partial n} N = BTN = BR^{-1}RD_N = D_u. \tag{5.2}$$

In particular, this equation implies that

$$\frac{\partial u}{\partial n} n = u,$$

which says that each phase volume is a homogeneous function of the first degree in the fluid composition. We also note that (4.1) and (5.2) imply that

$$\frac{\partial u}{\partial n} RB^{-1}\mathrm{v} = \mathrm{v}. \tag{5.3}$$

Analogous relationships also hold when the fluid is undersaturated. First we use (2.11) to compute

$$\frac{\partial \omega}{\partial n} = -\frac{1}{n^T(\partial \bar{f}/\partial \omega)}\bar{t}^T. \tag{5.4}$$

Then the matrix of partial phase volumes, computed from (2.19), is

$$\frac{\partial u}{\partial n} = Q\bar{B}\bar{T} + Q\frac{\partial \bar{B}}{\partial \omega}\bar{T}n\frac{\partial \omega}{\partial n}. \tag{5.5}$$

From equations (2.14) and (2.16), we know that the columns of N are orthogonal to $\partial\omega/\partial n$. As a result,

$$\frac{\partial u}{\partial n} N = Q\bar{B}\bar{T}N = Q\bar{B}\bar{T}\bar{R}\bar{D}_N Q^T = Q\bar{B}\bar{D}_N Q^T = D_u.$$

This proves that the homogeneity properties of the phases are true for undersaturated conditions as well. In this case we also have that (4.2) and the previous equation imply that

$$\frac{\partial u}{\partial n}\overline{RB}^{-1}Q^T\mathrm{v}=\mathrm{v}. \tag{5.6}$$

We can use the homogeneity relationships to rewrite the pressure equation (4.3) in the form

$$\frac{e^Tu-1}{\Delta t}\phi=\left[-\phi\, e^T\frac{\partial u}{\partial p}+e^Tu\frac{\partial \phi}{\partial p}\right]\frac{\partial p}{\partial t}+e^T\frac{\partial \mathrm{v}}{\partial x}-\frac{\partial}{\partial x}\left(e^T\frac{\partial u}{\partial n}\right)(ND_u^{-1}\mathrm{v}). \tag{5.7}$$

Now if we use Darcy's Law (3.1) to replace the phase velocities in (5.7) we obtain

$$\begin{aligned}&\frac{e^Tu-1}{\Delta t}\phi-\frac{\partial}{\partial x}\left(e^TL\rho\frac{\partial d}{\partial x}\kappa\right)+\frac{\partial}{\partial x}\left(e^T\frac{\partial u}{\partial n}\right)ND_u^{-1}L\rho\frac{\partial d}{\partial x}\kappa\\&\quad=\left[e^Tu\frac{\partial\phi}{\partial p}-\phi\, e^T\frac{\partial u}{\partial p}\right]\frac{\partial p}{\partial t}-\frac{\partial}{\partial x}\left(e^TLe\frac{\partial p}{\partial x}\right)+\frac{\partial}{\partial x}\left(e^T\frac{\partial u}{\partial n}\right)ND_u^{-1}Le\frac{\partial p}{\partial x}.\end{aligned} \tag{5.8}$$

The first two terms on the right-hand side of (5.8) are formally parabolic in structure. The total mobility e^TLe, which occurs in the term involving second-order spatial derivative of pressure, is positive. Thus, to show that the pressure equation is parabolic, we need only show that the coefficient of $\partial p/\partial t$ in (5.8) is positive.

5.2. Total fluid compressibility. In this section we show that the total rock-fluid system has negative compressibility, under the appropriate assumptions on the ratios R and formation volume factors B. This guarantees that the coefficient of $\partial p/\partial t$ in (5.8) is positive. We prove that this coefficient is the sum of two positive terms. First, as the pressure increases the rock occupies a smaller volume. Consequently, the porosity ϕ is a nondecreasing function and pressure; i.e., $\partial\phi/\partial p\geqq 0$. Thus the first term is positive. To show that the second term in the coefficient of $\partial p/\partial t$ is positive, we examine the pressure derivatives of u for fixed fluid composition n.

In the saturated case, u is a function of p and n given by (2.18). Thus

$$e^T\frac{\partial u}{\partial p}=e^T\frac{\partial BT}{\partial p}n=e^T\frac{\partial BT}{\partial p}RB^{-1}u.$$

We would like this quantity to be negative for all possible saturated mixtures. This desired behavior can be guaranteed only by placing additional restrictions on the formation volume factors B and ratios R. Since various values of n can produce arbitrary nonnegative values of u, we assume that B and R are chosen so that

$$e^T\frac{\partial BR^{-1}}{\partial p}RB^{-1}\leqq 0. \tag{5.9}$$

These inequalities essentially require that B and R interact properly, so that the fluid model is thermodynamically consistent. As a result of assumption (5.9), the total fluid volume cannot increase as pressure is increased; that is,

$$e^T\frac{\partial u}{\partial p}\leqq 0 \tag{5.10}$$

when the fluid is saturated.

When the fluid is undersaturated, the analysis is slightly more involved. We can use (2.19) to sum the pressure derivatives of the phase volumes:

$$e^T \frac{\partial u}{\partial p} = e^T Q \left[\frac{\partial \bar{B}}{\partial p} \bar{T} n + \frac{\partial \bar{B}}{\partial \omega} \bar{T} n \frac{\partial \omega}{\partial p} + \bar{B} \frac{\partial \bar{T}}{\partial p} n \right].$$

By a direct computation for each case of undersaturation we can show that

$$\frac{\partial \bar{T}}{\partial p} = \frac{\partial \bar{T}}{\partial p} Q \bar{T},$$

and

$$\frac{\partial \bar{B}}{\partial \omega} \bar{T} n \frac{\partial \omega}{\partial p} = -\frac{\partial \bar{B}}{\partial \omega} \frac{\partial \bar{T}}{\partial p} Q \bar{T} n \omega.$$

Using these relationships, we expand the pressure derivative of the total fluid volume:

$$0 \geqq e^T \frac{\partial u}{\partial p} = e^T Q \left[\frac{\partial \bar{B}}{\partial p} + \left(\bar{B} - \frac{\partial \bar{B}}{\partial \omega} \omega \right) \frac{\partial \bar{T}}{\partial p} Q \right] \bar{B}^{-1} Q^T u.$$

Since $Q^T u$ is nonnegative and arbitrary, it is sufficient to require that

$$0 \geqq e^T \left[\frac{\partial \bar{B}}{\partial p} + \left(\bar{B} - \frac{\partial \bar{B}}{\partial \omega} \omega \right) \frac{\partial \bar{T}}{\partial p} Q \right] B^{-1} \tag{5.11}$$

for all admissible values of ω and p.

Since inequality (5.10) is true for all black-oil models satisfying the compressibility conditions (5.9) (or (5.11) when the fluid is undersaturated), the coefficient of $\partial p / \partial t$ in (5.8) is the sum of two positive terms; hence, the pressure equation is parabolic. Note that because of the small compressibilities in typical fluids, we expect the pressure to reach a steady state quickly in the absence of changes in source terms.

5.3. Multiple spatial dimensions. The analysis of this section was performed in a single space dimension for simplicity of exposition. With minor changes in notation, such as replacing derivatives with respect to x with gradients and making v be an array of velocities of each phase in each coordinate direction, the same analysis shows that the pressure equation is parabolic in multiple spatial dimensions. This is because the essential points in the argument involve thermodynamic properties, such as partial volumes and compressibilities, that are independent of the number of spatial coordinates.

6. Characteristic analysis. In this section, we analyze the component conservation equations to show that they are hyperbolic. We also compute the right (and left) eigenvectors of the linearized flux. These eigenvectors provide information about the structure of the wave fields and are used by the numerical method discussed in § 7. (Note that to obtain the wave speeds from the eigenvalues of the linearized flux, we must multiply by $1/\phi$ because of the natural scaling in the system.) At several stages in the computation of the eigenvalues we use deflation to reduce the system. In some cases we assume that the system does not exhibit eigenvector deficiences in order to perform the deflation. The importance of these eigenvector deficiencies and their numerical treatment is discussed in [5].

6.1. Saturated conditions. If we write the conservation law (4.5) in quasilinear form, we have

$$\frac{\partial n \phi}{\partial t} + \frac{\partial h}{\partial n} \frac{\partial n}{\partial x} = 0.$$

For the purposes of the characteristic analysis, we consider p (and consequently ϕ) and v_T to be independent of n. As a result, they enter the characteristic analysis as spatially dependent terms that can be frozen for the analysis. Thus, the system is hyperbolic if and only if

$$H \equiv \frac{\partial h}{\partial n}$$

has real eigenvalues for all values of n. This condition is straightforward to verify when the fluid is saturated. In multiple spatial dimensions, the system of conservation laws is hyperbolic if and only if the partial derivatives of the flux in any given direction, taken with respect to the conserved quantities, has only real eigenvalues. The analysis to follow can therefore be trivially modified to handle fluid flow in multiple spatial dimensions as well. We have omitted these complications in order to simplify the exposition.

Equation (4.6) shows that the component flux vector for saturated flow is $h = RB^{-1}v$. In this expression, R and B are independent of n. The vector of phase velocities v is a function of n only through the saturations. Thus, the definition (3.2) of the saturations shows that

$$\frac{\partial v}{\partial n} = \frac{\partial v}{\partial s}\frac{\partial s}{\partial n} = \frac{\partial v}{\partial s}[I - s\,e^T]\frac{\partial u}{\partial n}\frac{1}{e^T u}.$$

As a result, it is easy to show that the component derivatives of the flux satisfy

$$H\,e^T u = RB^{-1}\frac{\partial v}{\partial s}[I - s\,e^T]BR^{-1}.$$

In other words, $H\,e^T u$ is similar to the matrix

$$V \equiv \frac{\partial v}{\partial s}[I - s\,e^T].$$

This is the same matrix that appears in the characteristic analysis of the Buckley–Leverett model [4]. The similarity transformation essentially maps from component densities to saturations.

The sum of the phase velocities is the total velocity, which is independent of n. As a result, we have

$$e^T V = 0.$$

Thus, e is a left eigenvector of V with eigenvalue zero. We use this eigenvector to deflate V as follows:

$$\begin{bmatrix} 1 & e^T \\ 0 & I \end{bmatrix} V \begin{bmatrix} 1 & -e^T \\ 0 & I \end{bmatrix} = \begin{bmatrix} 0 & 0 \\ c & C \end{bmatrix},$$

where the 2×2 matrix C and the 2-vector c are defined by

$$C \equiv [0 \quad I]\frac{\partial v}{\partial s}\begin{bmatrix} 0 \\ I \end{bmatrix}, \qquad c \equiv -C[0 \quad I]s.$$

Thus the remaining eigenvalues of $H\,e^T u$ are eigenvalues of C.

These two eigenvalues are the same as in a three-phase incompressible flow problem. This relationship of saturated flow to incompressible flow indicates that the hyperbolicity of the saturated system is inherited from the relative permeability model.

In other words, the characteristic speeds are independent of the compressibility and mass transfer effects that complicate the black-oil model. For this reason we will simply assume that these eigenvalues are real. This is generally the case, but there are examples to the contrary (see [4]). Thus, we assume that we can find a real nonsingular matrix X_C and a real diagonal matrix Λ_C so that

$$CX_C = X_C \Lambda_C. \tag{6.1}$$

We also ignore for the moment the possibility that the two eigenvalues of C may coincide at some point and that C may have an eigenvector deficiency. Thus we assume that we can solve

$$X_C \Lambda_C a = c \tag{6.2}$$

for the vector a. Then the right eigenvectors of $H e^T u$ are the columns of

$$X \equiv RB^{-1} \begin{bmatrix} 1 & -e^T \\ 0 & I \end{bmatrix} \begin{bmatrix} 1 & 0 \\ 0 & X_C \end{bmatrix} \begin{bmatrix} 1 & 0 \\ -a & I \end{bmatrix}, \tag{6.3}$$

and the left eigenvectors are easily determined by inverting this expression. In summary, we have shown that

$$HX = X\Lambda,$$

where

$$\Lambda = \begin{bmatrix} 0 & 0 \\ 0 & \Lambda_C(1/e^T u) \end{bmatrix}.$$

Thus, the wave speeds associated with the linearized flux are zero and "Buckley-Leverett" modes corresponding to the diagonal entries of Λ_C.

Only one Riemann invariant is known to us for saturated flow. In fact, it is easy to see that the volume discrepancy error $1 - e^T u$ is a Riemann invariant corresponding to the zero eigenvalue. This degenerate, linear advection mode is the false wave that is introduced by the sequential splitting.

6.2. Three-component two-phase flow. When all three phases exist, the thermodynamic behavior of the black-oil model essentially factors out of the characteristic analysis, and we are left with characteristic speeds that are specified by the relative permeability model. In the undersaturated case, the dependence of the flux on the undersaturation parameter ω introduces some additional complication into the analysis, as well as a new wave speed.

The undersaturated flux, given by (4.7), can be written as

$$h = \overline{RB}^{-1} \bar{v}, \tag{6.4}$$

where $\bar{v} = Q^T v$. If we now differentiate the flux as given by (6.4), we obtain

$$H \equiv \frac{\partial h}{\partial n} = \frac{\partial \overline{RB}^{-1}}{\partial \omega} \bar{v} \frac{\partial \omega}{\partial n} + \overline{RB}^{-1} \frac{\partial \bar{v}}{\partial n}.$$

Using the characteristic analysis of saturated flow as motivation, we want to separate, to the greatest extent possible, the thermodynamics of the fluid from the fluid flow. As in the saturated case, we seek a similarity transform of H to accomplish this task.

Recalling (5.4) for the component derivatives of ω and (2.14) for the orthogonality of $\bar{t}$ with the columns of $\bar{R}$, it is easy to show that $\bar{t}^T$ is a left eigenvector of the linearized flux. This observation suggests that an appropriate similarity transform is defined by

$$X_M^{-1} = \begin{bmatrix} \bar{B}\bar{T} \\ \bar{t}^T \end{bmatrix},$$

with inverse

$$X_M = [\overline{RB}^{-1}, q].$$

(Actually, X_M can be derived as the matrix of right eigenvectors for the matrix M of component derivatives of the vector of components in the aqueous phase.) If we apply this transformation to $H \equiv \partial h/\partial n$, we obtain

$$X_M^{-1} H X_M = \begin{bmatrix} \bar{V} & \overline{BT}Hq \\ 0 & \lambda \end{bmatrix}$$

where

$$\bar{V} = \frac{\partial \bar{\mathrm{v}}}{\partial n}\overline{RB}^{-1},$$

and

$$\lambda = \bar{t}^T \frac{\partial \overline{RB}^{-1}}{\partial \omega}\bar{\mathrm{v}}\frac{\partial \omega}{\partial n}q. \tag{6.5}$$

If we expand the expression for the eigenvalue λ we find that

$$\lambda = \frac{\dfrac{R_l'(p_b)}{B_l(p,p_b)}\mathrm{v}_l + \dfrac{R_a'(p_b)}{B_a(p,p_b)}\mathrm{v}_a}{R_l'(p_b)n_o + R_a'(p_b)n_w} = \frac{R_l' n_o \dfrac{\mathrm{v}_l}{u_l} + R_a' n_w \dfrac{\mathrm{v}_a}{u_a}}{R_l' n_o + R_a' n_w}$$

when the vapor phase is missing, and

$$\lambda = \frac{\mathrm{v}_v}{B_v n_g} = \frac{\mathrm{v}_v}{u_v}$$

when the liquid phase is missing. For each phase, v_p/u_p is the particle velocity within that phase. Therefore, λ corresponds to a weighted sum of particle velocities. Furthermore, its corresponding left eigenvector is the third row of X_M^{-1}, which is proportional to $\partial\omega/\partial n$. In other words, the undersaturation variable $\omega = p_b$ or $\bar{R}_v$ is a Riemann invariant.

The remaining eigenvalues of H are eigenvalues of the 2×2 matrix $\bar{V}$. This matrix involves component derivatives of $\bar{\mathrm{v}}$, which in turn depends on n through ω and the saturations of the existing phases. Accordingly, we define the vector of saturations in the existing phases by

$$\bar{s} = \frac{\bar{u}}{e^T\bar{u}}$$

where $\bar{u} = \overline{BT}n$ is the vector of partial phase volumes of the existing phases. Applying

the chain rule, we obtain

$$\frac{\partial \bar{v}}{\partial n} = \left(\frac{\partial \bar{v}}{\partial \omega} + \frac{\partial \bar{v}}{\partial \bar{s}} \frac{\partial \bar{s}}{\partial \bar{u}} \frac{\partial \bar{u}}{\partial \omega} \right) \frac{\partial \bar{\omega}}{\partial n} + \frac{\partial \bar{v}}{\partial \bar{s}} \frac{\partial \bar{s}}{\partial \bar{u}} \frac{\partial \bar{u}}{\partial n}.$$

Equation (5.5) and the orthogonality relations for undersaturated flow give

$$\bar{V} = \frac{\partial \bar{v}}{\partial \bar{s}} [I - s e^T] \frac{1}{e^T \bar{u}}.$$

Thus the matrix $\bar{V}$ corresponds to the linearization of two-phase Buckley–Leverett flow.

Its eigenvalues are easily determined using the same procedure as was used to analyze saturated flow in the previous section. In particular, we know that these eigenvalues are zero and the saturation derivative of the aqueous phase velocity. Thus, we define

$$X_{\bar{V}} \equiv \begin{bmatrix} s_* & -1 \\ s_a & 1 \end{bmatrix},$$

where s_* is the saturation of the other existing phase, and

$$\Lambda_{\bar{V}} \equiv \begin{bmatrix} 0 & 0 \\ 0 & \partial v_a / \partial s_a \end{bmatrix}.$$

Then the columns of $X_{\bar{V}}$ are right eigenvectors of $\bar{V}$:

$$\bar{V} X_{\bar{V}} = X_{\bar{V}} \Lambda_{\bar{V}}.$$

(Here, we note that $\bar{V}$ cannot have an eigenvector deficiency.) We let a solve

$$X_{\bar{V}} \left(\Lambda_{\bar{V}} a \frac{1}{e^T u} - a\lambda \right) = \bar{B} \bar{T} H q, \tag{6.6}$$

where we assume for the moment that the eigenvalues of $\bar{V}$ are distinct from $\lambda\, e^T u$. Then the right eigenvectors of H are the columns of

$$X \equiv X_M \begin{bmatrix} X_{\bar{V}} & 0 \\ 0 & 1 \end{bmatrix} \begin{bmatrix} I & -a \\ 0 & 1 \end{bmatrix}. \tag{6.7}$$

It is easy to invert this expression to obtain the left eigenvectors of H. We have shown that the eigenvectors and eigenvalues of H are given by

$$HX = X\Lambda,$$

where

$$\Lambda = \begin{bmatrix} \Lambda_{\bar{V}} (1/e^T u) & 0 \\ 0 & \lambda \end{bmatrix}. \tag{6.8}$$

The eigenvalues of H are the previously cited average of the particle velocities of the phases, zero, and the Buckley–Leverett mode $\partial v_a / \partial s_a$.

Except for the case when gas dissolves in liquid and aqua simultaneously and the vapor phase is missing, the left eigenvector corresponding to the zero eigenvalue is the vector of component derivatives of the volume discrepancy error $1 - e^T u$. Thus in almost all cases, the volume discrepancy error is the Riemann invariant corresponding to the degenerate wave for undersaturated flow as well. Recall that the undersaturation

variable $\omega = p_b$ or $\bar{R}_v$ is also a Riemann invariant corresponding to the average λ of the particle velocities defined by (6.5).

6.3. Continuity of the eigenstructure. As long as the flow remains saturated, the eigenvalues and eigenvectors of the flux derivatives will be continuously varying, provided all of the functions used to describe the black-oil model are continuously differentiable. Similarly, if the flow continues to have the same phase missing due to undersaturation, the eigenstructure of the conservation law will be continuous. However, when the flow exhibits a phase change, then the inherent discontinuities in the derivatives of the formation volume factors and the ratios force the eigenvalues and eigenvectors to be discontinuous. This can be easily seen from the characteristic analysis. For saturated flow, the eigenvalues are zero and the two nontrivial derivatives of the saturation derivatives of the phase velocities. For undersaturated flow, zero and the saturation derivative of the aqueous phase velocity are still eigenvalues. However, the third eigenvalue is a weighted average of the particle velocities in the two phases. This third eigenvalue is generally discontinuous across a phase change. The eigenvectors are also discontinuous.

7. Numerical examples. The bulk of this paper has concerned the development and analysis of a sequential formulation of the black-oil flow equations. To obtain a quantitative description of the types of fronts that can form and propagate, we are essentially forced to use a numerical approximation. Of course, some information can be obtained by freezing coefficients in the component conservation equations and studying the associated Riemann problems. However, in realistic flow situations, the fluid velocity depends on the pressure gradient so that if pressure is constant nothing flows. Thus, the Riemann problems give only an approximation to true flow behavior. Nevertheless, we will use concepts drawn from the theory of hyperbolic conservation laws to interpret numerical results.

Since the objective of this section is to study the behavior of the black-oil system and not to advocate any particular numerical method, our description of the computational procedure will be very brief. We discretize the pressure equation (4.3) using a block-centered finite difference approximation analogous to the lowest-order mixed finite-element method. Theoretical properties of this approach are discussed by Weiser and Wheeler [14]. This approach was also used to solve in the pressure equation in Bell, Shubin, and Trangenstein [3]. The interested reader is referred to these works for details.

The discretization of the component conservation equations is somewhat more problematic. To provide accurate resolution of sharp fronts requires a higher-order method, even on relatively fine grids. However, second-order linear schemes typically do not perform well on conservation laws that are not both strictly hyperbolic and genuinely nonlinear. For this reason we use a second-order Godunov method for discretization of the component conservation equations (4.5)-(4.7). The particular form of the scheme is based on ideas presented by Colella [6] and is discussed in some detail in Bell, Shubin, and Trangenstein [3]. Although, in general, Godunov methods require some type of approximate Riemann problem solution, in this paper we consider only numerical examples that do not include gravitational effects. (Bell, Colella, and Trangenstein [5] discussed approximations to the Riemann problem suitable for use with second-order Godunov methods and applied this methodology to black-oil simulation with gravitational effects in one and two space dimensions.) Under these circumstances, the Riemann problem solutions needed for the numerical method

trivialize to a simple upwind determination. Timestep control is based on CFL considerations for the component conservation equations. The details of this procedure were also discussed in [3].

The discussion of numerical examples is broken into three parts. First, we consider flow entirely within the saturated region, i.e., all three-phases are present. Next, we study the behavior of various undersaturated flow regimes. Finally, two examples are given that illustrate the behavior of the solution when pressure and fluid composition result in an interaction of saturated and undersaturated flow regimes.

All of the computations are performed for a homogeneous linear reservoir 1,000 feet long with no dip. The computational results deal with the most general case of mass transfer with volatile oil and gas dissolving in both liquid and aqueous phases. The remaining reservoir and fluid properties are given explicitly in Appendix A. The computations are performed with 200 grid cells so that fronts may be accurately resolved.

7.1. Saturated flow example. For saturated flow the characteristic speeds are determined by an analogous three-phase incompressible flow problem. Provided that the characteristic directions do not coalesce and that the characteristic speeds are real, saturated flow is strictly hyperbolic. However, none of the wave modes are genuinely nonlinear. Thus, for each nontrivial wave family we have the possibility of a compound wave composed of a rarefaction and a shock. Our first example provides a realization of this phenomena. The initial component densities in the reservoir and the injected component densities are given by

$$n_R = \begin{pmatrix} 0.703 \\ 70.30 \\ 0.0502 \end{pmatrix} \quad \text{and} \quad n_I = \begin{pmatrix} 0.0414 \\ 66.23 \\ 0.497 \end{pmatrix},$$

respectively. The initial reservoir pressure is 1,800 psi; we inject at 2,000 psi and produce at 1,600 psi. In Fig. 1(a), we plot density versus distance along the reservoir for each of the components. Figure 1(b) contains corresponding plots of saturations as well as the eigenvalues of the linearized flux function. In the saturation plot, the lower curve is the vapor saturation and the upper curve is the sum of the vapor saturation and the liquid saturation. Thus, the distance between the lower curve and the upper curve represents the liquid saturation and the distance from the upper curve to the top of the graph represents the aqueous saturation. We do not plot the zero eigenvalue corresponding to the fictitious wave introduced by the splitting. The two Buckley-Leverett-type waves are readily apparent in these figures. The graph of the eigenvalues shows that the slower Buckley-Leverett mode forms a rarefaction starting at $x = 50$, continuing up to a shock at $x = 150$. The faster Buckley-Leverett mode forms a rarefaction at $x = 425$, connecting to a shock at $x = 725$. (The minor decrease in the larger eigenvalue near $x = 400$ cannot be explained in terms of hyperbolic wave behavior; it may represent some type of pressure effect.) The component behavior from $x = 725$ to the production well is due to pressure effects, since the flow history shows that the injected materials have not yet progressed past $x = 725$. In order to properly interpret the eigenvalue graphs, we have multiplied the eigenvalues by $1/\phi$ to obtain the wave speeds.

7.2. Undersaturated flow examples. The undersaturated flow regime exhibits somewhat more interesting behavior. The additional complication in the wave structure introduced by the volume discrepancy splitting makes rigorous analysis of the wave

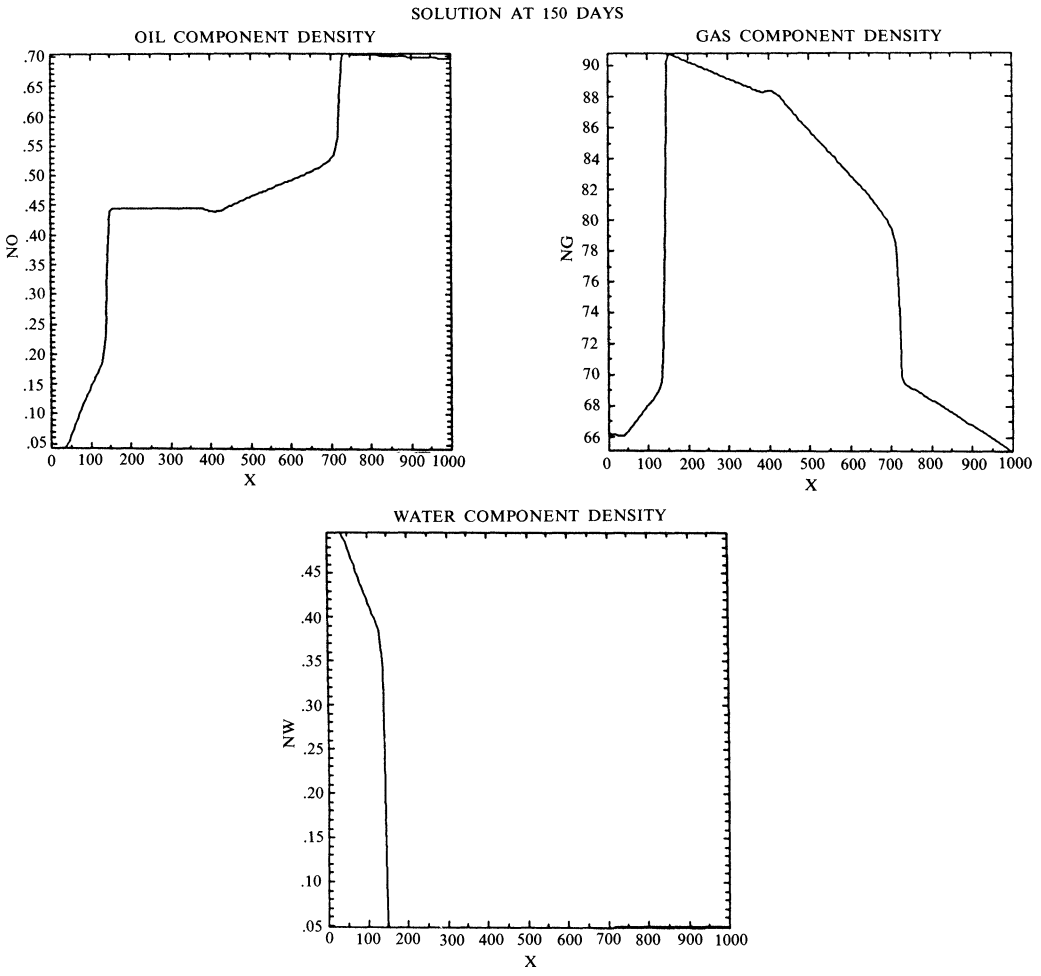

FIG. 1(a). *Component densities for saturated flow example.*

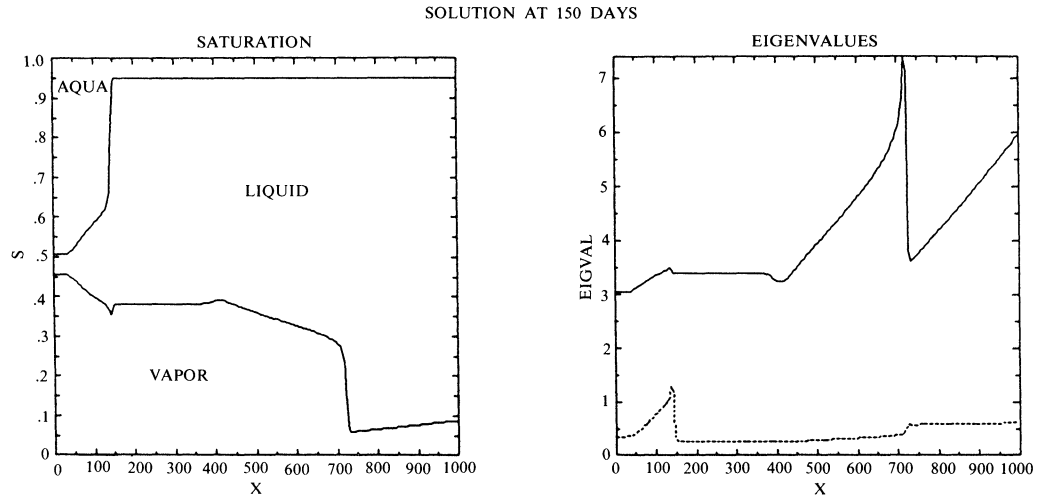

FIG. 1(b). *Saturations and wave speeds for saturated flow example.*

structure difficult. However, if we assume there is no mass transfer, the component conservation equations take roughly the same form as the system considered by Keyfitz and Kranzer [10] and by Isaacson [8]. In those papers one wave family is nonlinear but the other is linearly degenerate. Although our situation is more complex, by analogy we expect to see similar types of behavior for undersaturated flow.

Our first example contains no liquid phase. We inject a two-phase vapor-aqua mixture into an undersaturated vapor reservoir. The initial component densities in the reservoir and the injected component densities are given by

$$n_R = \begin{pmatrix} 0.0258 \\ 258.17 \\ 0.0 \end{pmatrix} \quad \text{and} \quad n_I = \begin{pmatrix} 0.00046 \\ 45.67 \\ 0.9135 \end{pmatrix},$$

respectively. The initial reservoir pressure is 4,200 psi; we inject at 4,300 psi and produce at 4,100 psi. For this case, the component conservation equations (with pressure and total velocity fixed, and zero volume discrepancy) are of exactly the same form as the system considered by the above authors. Component densities are plotted in Fig. 2(a) with saturations and eigenvalues in Fig. 2(b). Of course, in this case the two saturation curves coincide because there is no liquid. The eigenvalue corresponding to the particle velocity is plotted with a dotted line. For this example the leading wave is again a rarefaction-shock Buckley–Leverett wave. We also note a discontinuous jump in oil density around 200 feet. As can be seen from the eigenvalue plot, this wave corresponds to a contact discontinuity in the particle-velocity family.

For our next example we inject a two-phase mixture with the vapor phase missing into an undersaturated liquid-aqua reservoir. The initial component densities in the reservoir and the injected component densities are given by

$$n_R = \begin{pmatrix} 0.734 \\ 32.10 \\ 0.1835 \end{pmatrix} \quad \text{and} \quad n_I = \begin{pmatrix} 0.404 \\ 4.042 \\ 0.647 \end{pmatrix},$$

respectively. The initial reservoir pressure is 1,200 psi; we inject at 1,400 psi and produce at 1,000 psi. Component densities, saturations, and eigenvalues for this case are plotted in Figs. 3(a) and 3(b). Although the equations are not directly analogous to the Keyfitz–Kranzer system, we nevertheless see a Buckley–Leverett type wave followed by a slower contact discontinuity in the particle velocity family.

In the examples presented thus far, the wave speeds have remained nicely separated. This need not be the case. In the next example we inject an undersaturated aqueous phase into a reservoir containing an undersaturated liquid phase. The initial component densities in the reservoir and the injected component densities are given by

$$n_R = \begin{pmatrix} 0.834 \\ 58.39 \\ 0.0 \end{pmatrix} \quad \text{and} \quad n_I = \begin{pmatrix} 0.0 \\ 4.34 \\ 1.084 \end{pmatrix},$$

respectively. The initial reservoir pressure is 1,800 psi; we inject at 2,000 psi and produce at 1,600 psi. Computational results for this case are plotted in Figs. 4(a) and 4(b). The wave structure is somewhat more complex in this case. Note that at roughly 300 feet the two eigenvalues cross. At the point where they cross we see a contact discontinuity in the particle-velocity family connecting to a faster moving Buckley–Leverett rarefaction shock. The slow-moving rarefaction from 0–50 feet is another wave in the Buckley–Leverett family. Again, behavior of this type is similar to behavior obtained by Keyfitz and Kranzer and by Isaacson.

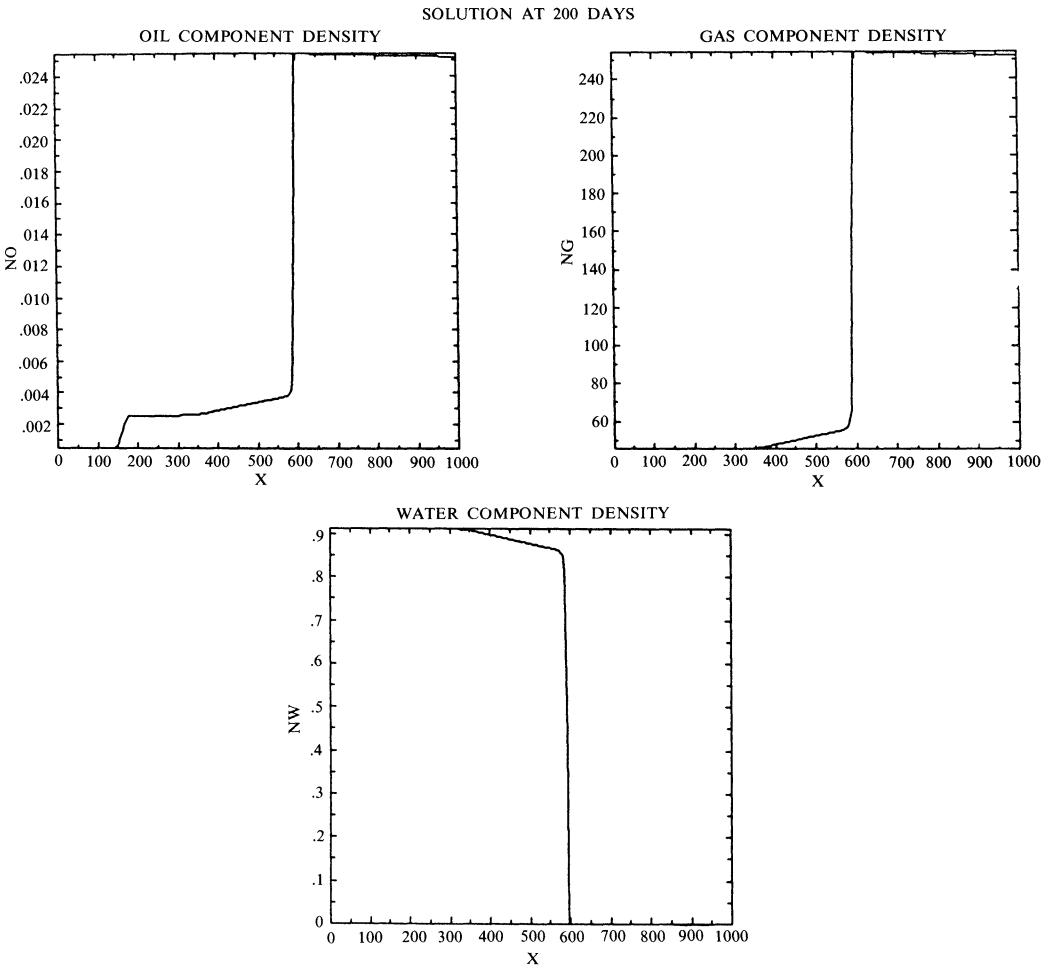

FIG. 2(a). *Component densities for first undersaturated flow example.*

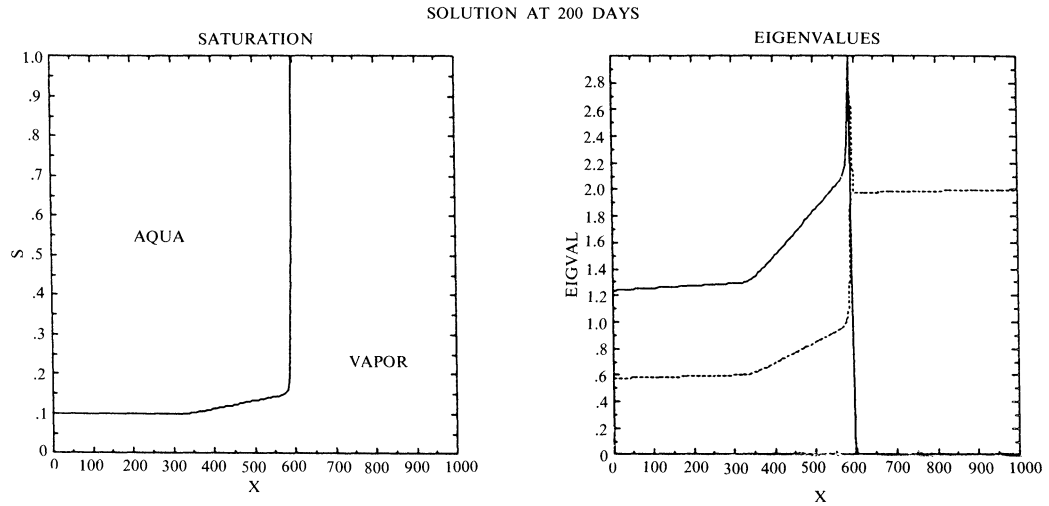

FIG. 2(b). *Saturations and wave speeds for first undersaturated flow example.*

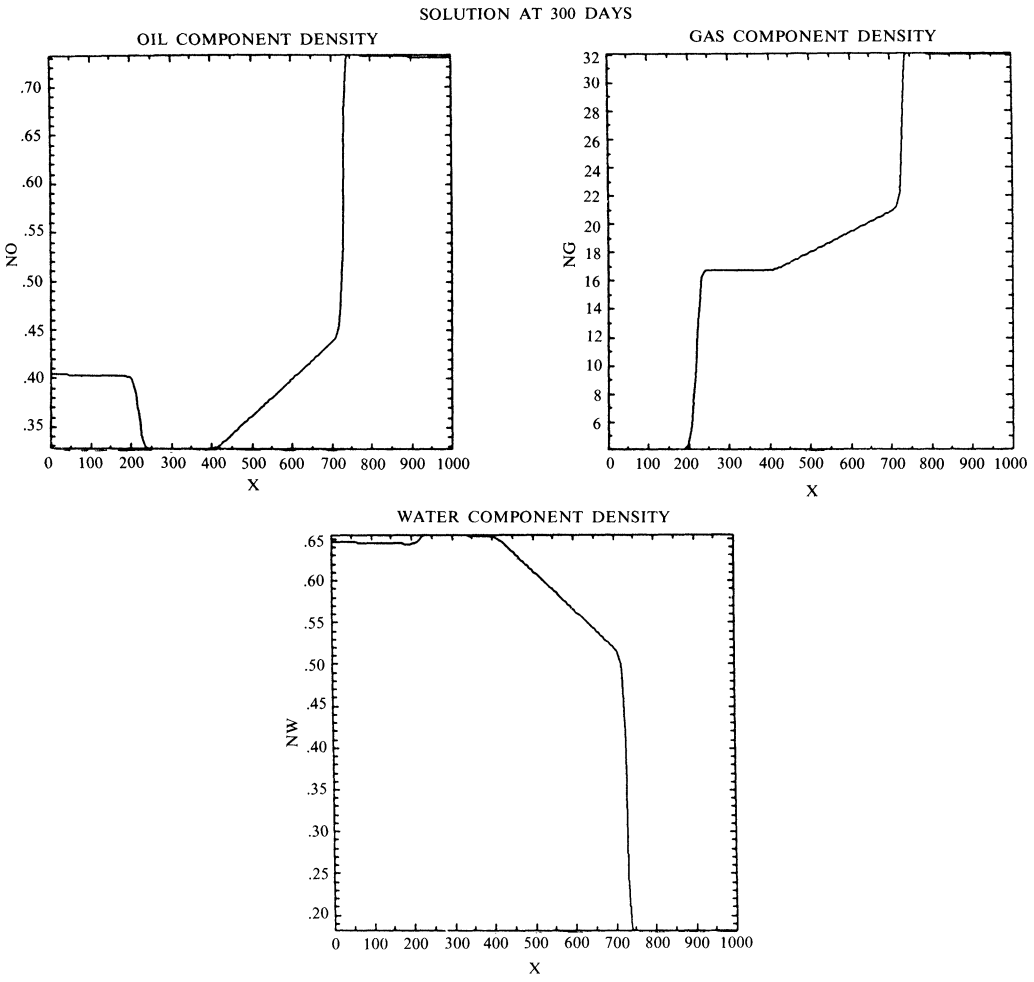

FIG. 3(a). *Component densities for second undersaturated flow example.*

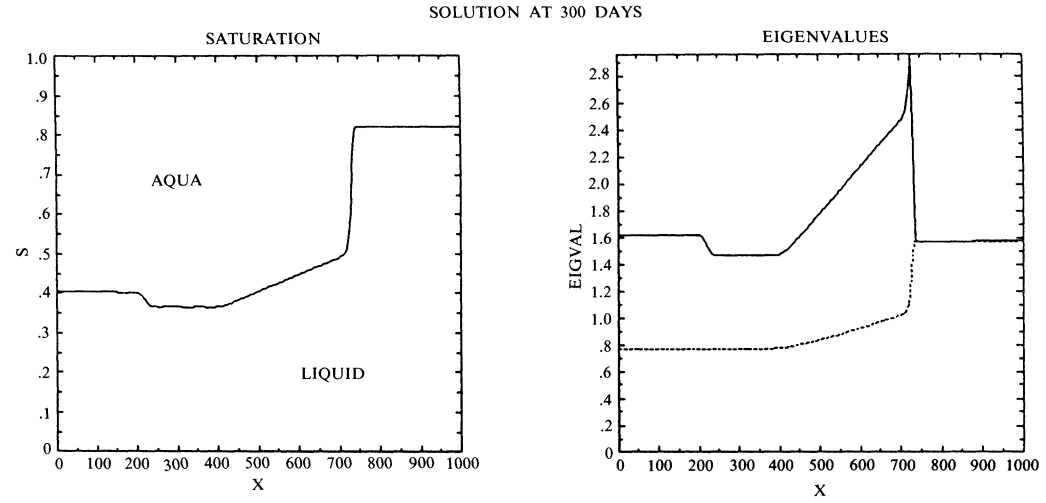

FIG. 3(b). *Saturations and wave speeds for second undersaturated flow example.*

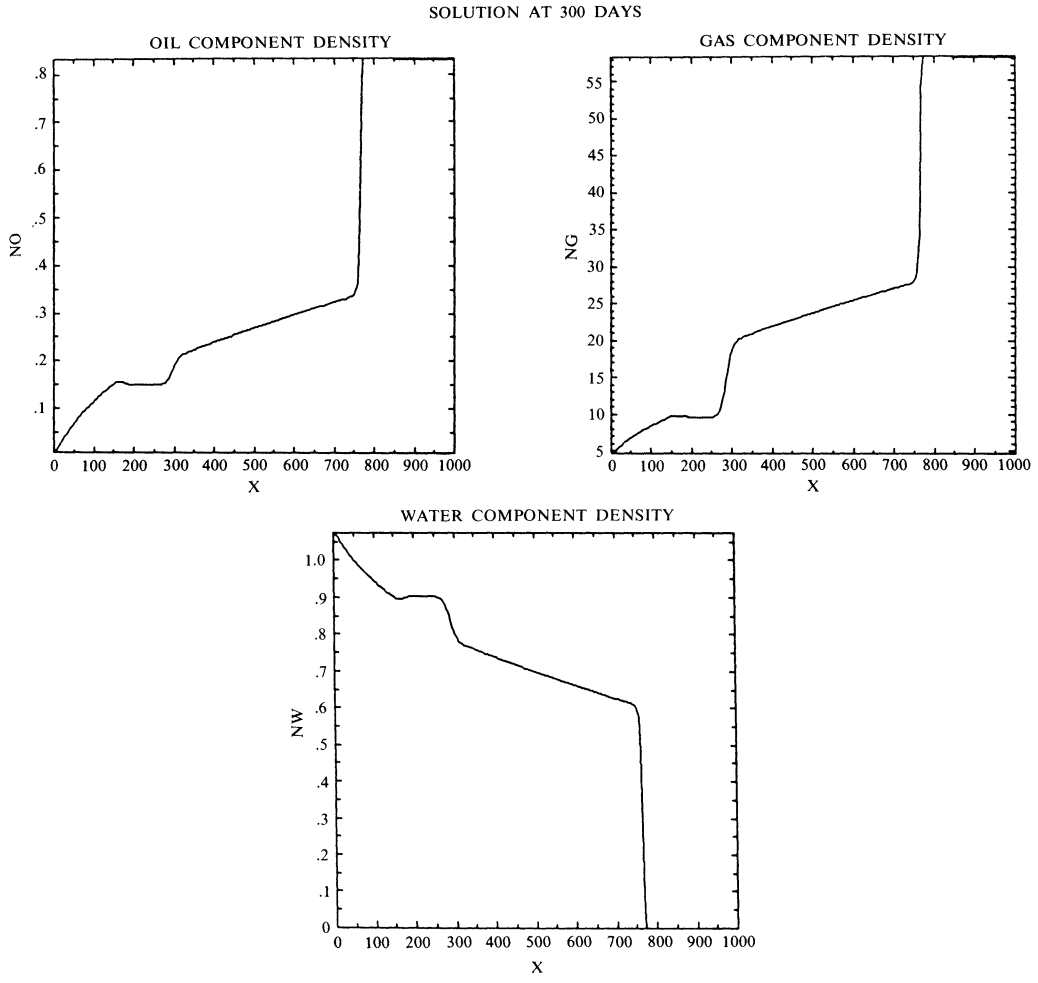

FIG. 4(a). *Component densities for third undersaturated flow example.*

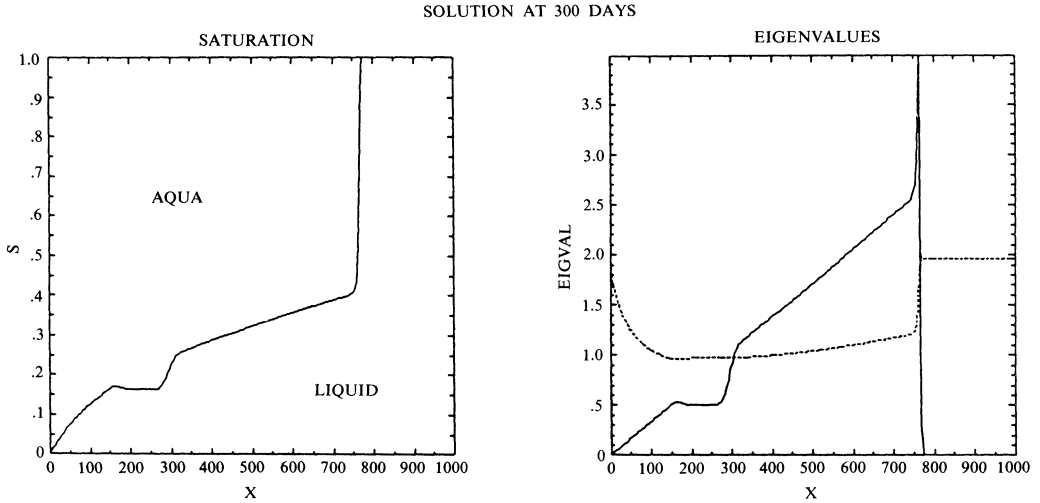

FIG. 4(b). *Saturations and wave speeds for third undersaturated flow example.*

7.3. Additional examples. The above examples have demonstrated that when the flow remains in one particular regime, the behavior of the waves can be reasonably well understood from the hyperbolic structure of the component conservation equations. However, composition and pressure changes can create flows that mix saturated and undersaturated flows. In this section, we consider two such complex flow situations.

In the first example we illustrate behavior caused by dramatic composition changes. Here, we inject a two-phase mixture with the liquid phase missing into a two-phase undersaturated reservoir with the vapor phase missing. The initial component densities in the reservoir and the injected component densities are given by

$$n_R = \begin{pmatrix} 0.668 \\ 100.19 \\ 0.0668 \end{pmatrix} \quad \text{and} \quad n_I = \begin{pmatrix} 0.0179 \\ 178.68 \\ 0.647 \end{pmatrix},$$

respectively. The initial reservoir pressure is 4,200 psi; we inject at 4,300 psi and produce at 4,100 psi. Component densities, saturations and eigenvalues are plotted in Figs. 5(a) and 5(b). Note that in this case the solution contains a three-phase region connecting the two undersaturated regions. The fastest wave is clearly a Buckley–Leverett rarefaction-shock pattern moving into the relatively undisturbed reservoir. There is also another discontinuity connecting the injection mixture to the three-phase region.

Our final example shows the effect of pressure variation on the flow. This example typifies a waterflood example in which water containing no hydrocarbons is injected into a reservoir containing an undersaturated liquid. The initial component densities in the reservoir and the injected component densities are given by

$$n_R = \begin{pmatrix} 0.646 \\ 116.29 \\ 0.00 \end{pmatrix} \quad \text{and} \quad n_I = \begin{pmatrix} 0.0 \\ 0.0 \\ 1.271 \end{pmatrix},$$

respectively. The initial reservoir pressure is 3,500 psi; we inject at 4,000 psi and produce at 3,000 psi. Computational results after 50 days of injection are shown in Figs. 6(a) and 6(b). In the left part of the reservoir we observe a contact-rarefaction-shock pattern similar to Figs. 3(a), 3(b). It is interesting to note that, although there is a liquid phase capable of containing gas in the left portion of the reservoir, nevertheless, all of the gas is swept from this area. In the right part of the reservoir we see a vapor phase that forms because the production pressure drops the reservoir pressure below the bubble point. (Of course, the eigenvalues are not directly useful in analyzing this pressure-dependent effect.) In Figs. 7(a) and 7(b), we show computational results after 125 days of injection. Of particular note here is the gas bubble that forms from the interaction of the advancing fronts and from the free gas in the vapor phase that forms from the pressure drop.

8. Concluding remarks. In this paper we have presented and analyzed a volume-discrepancy formulation of the equations governing black-oil reservoir simulation. This splitting decoupled the system into a parabolic pressure equation and a system of hyperbolic conservation laws. Using the splitting as a basis for a sequential numerical method, we have studied the types of fronts that can propagate through the system. The numerical results indicate that when the flow remained within one of three regimes (saturated, undersaturated liquid-aqua, or undersaturated vapor), the hyperbolic structure of the component conservation equations provided an excellent description of much of the flow behavior. In particular, for saturated flow we found two nonlinear modes of wave propagation, each of which was capable of generating compound wave

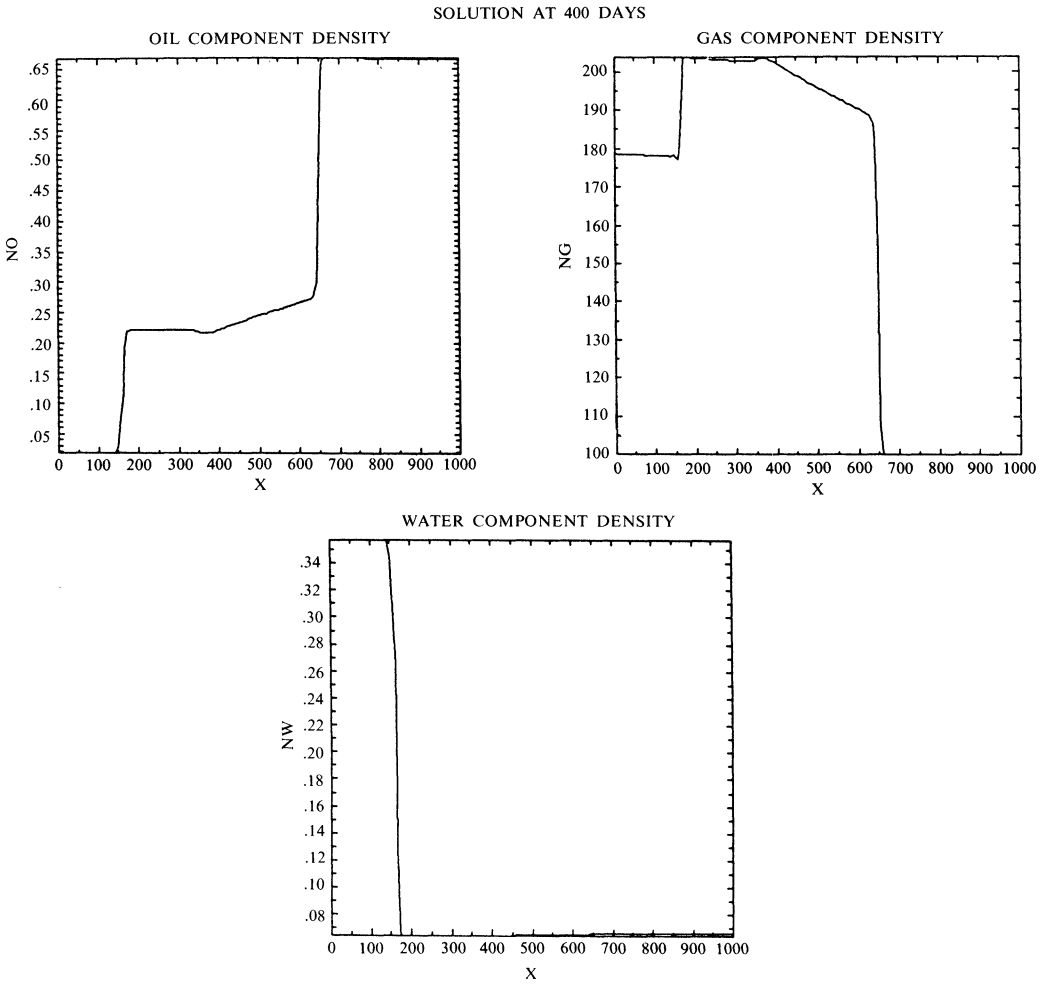

FIG. 5(a). *Component densities for first mixed flow example.*

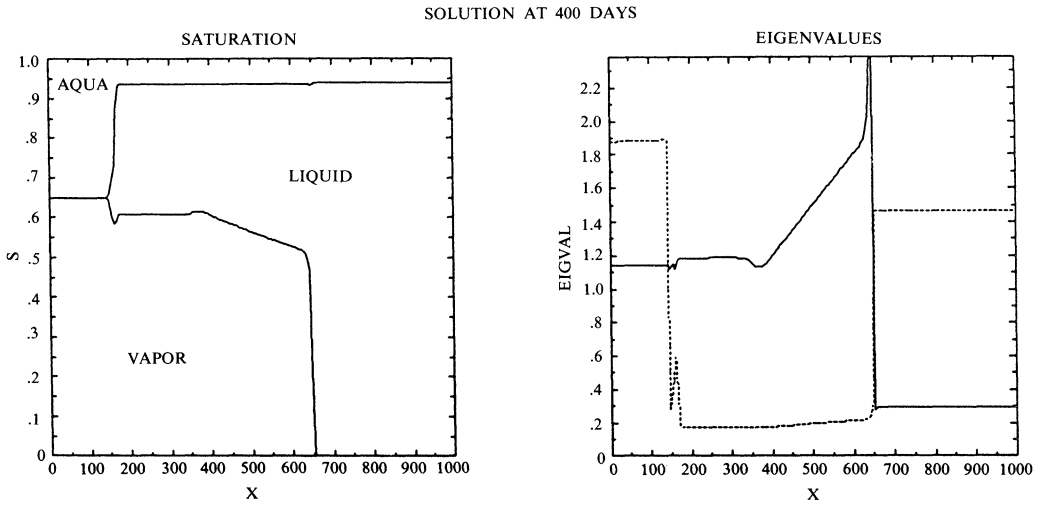

FIG. 5(b). *Saturations and wave speeds for first mixed flow example.*

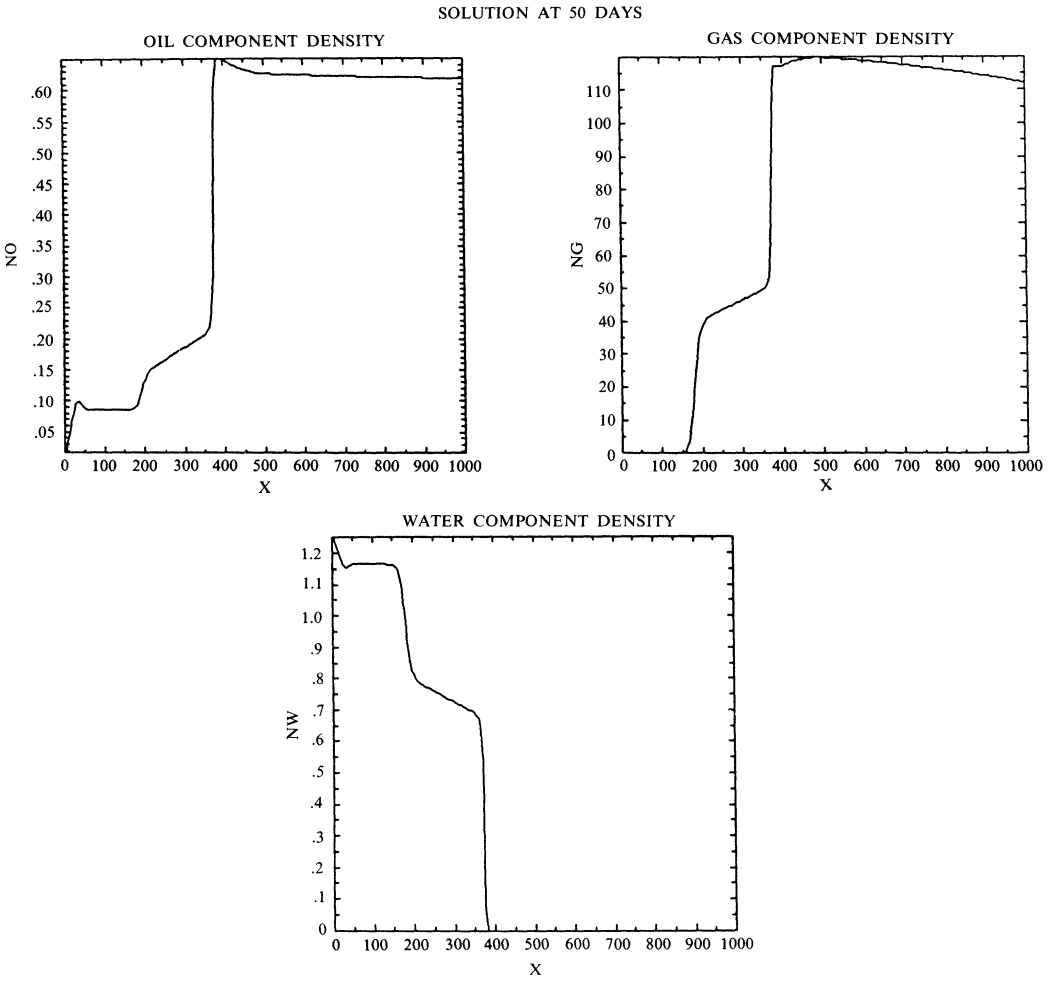

FIG. 6(a). *Component densities for second mixed flow example at early time.*

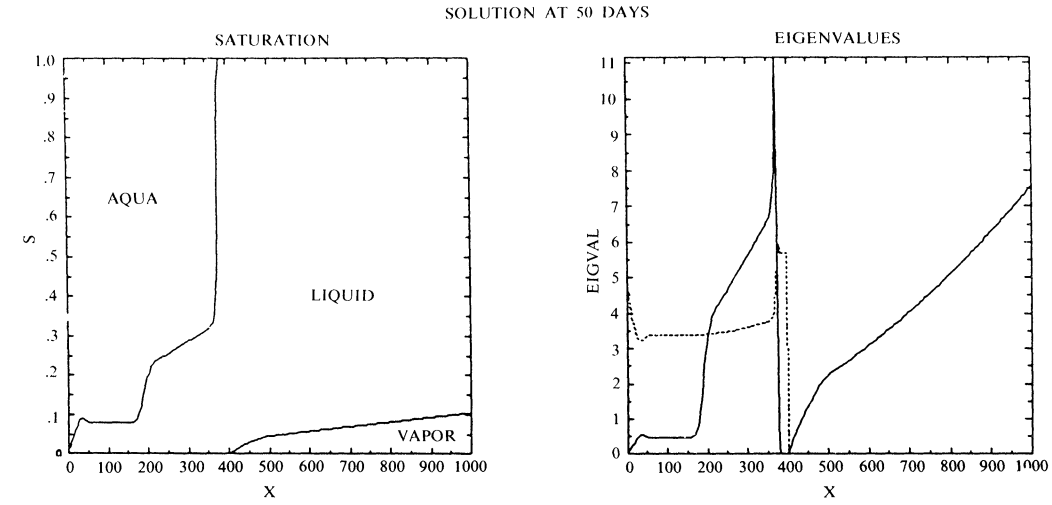

FIG. 6(b). *Saturations and wave speeds for second mixed flow example at early time.*

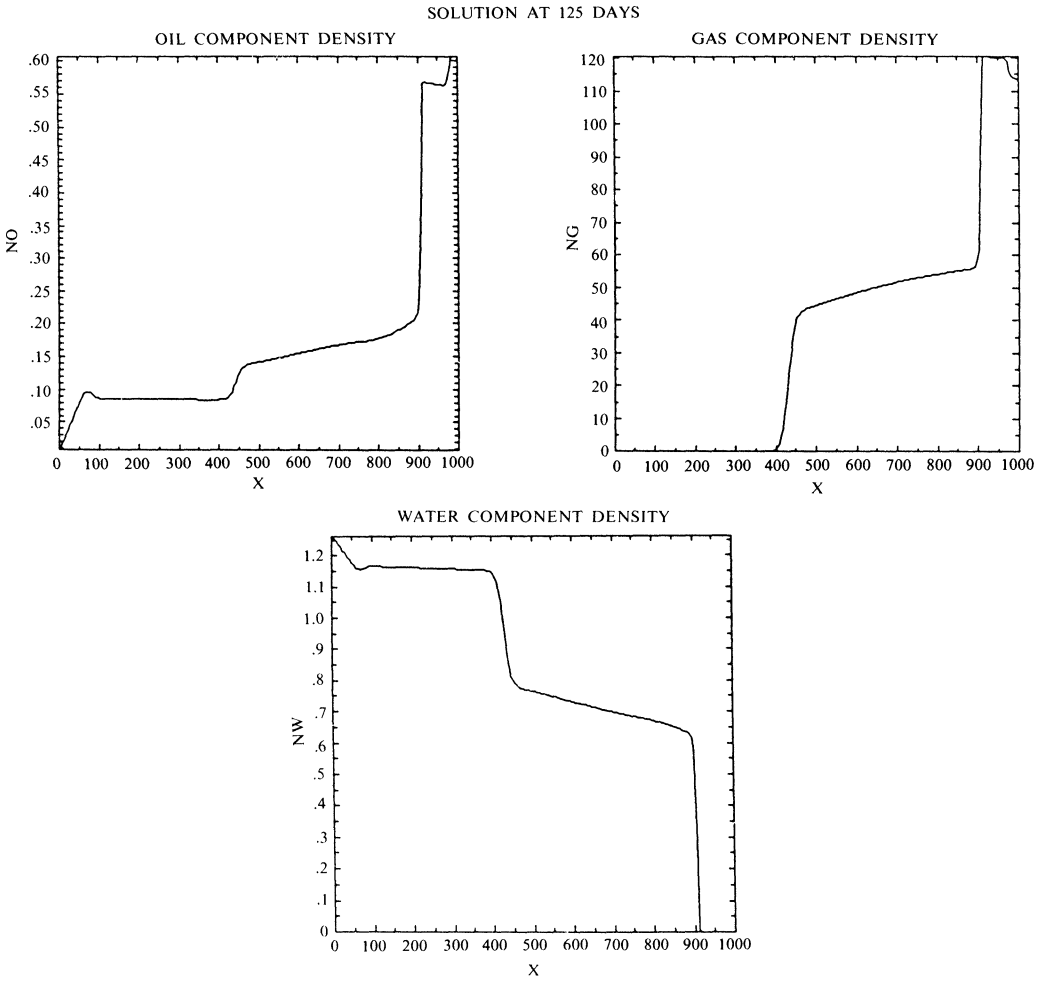

FIG. 7(a). *Component densities for second mixed flow example at late time.*

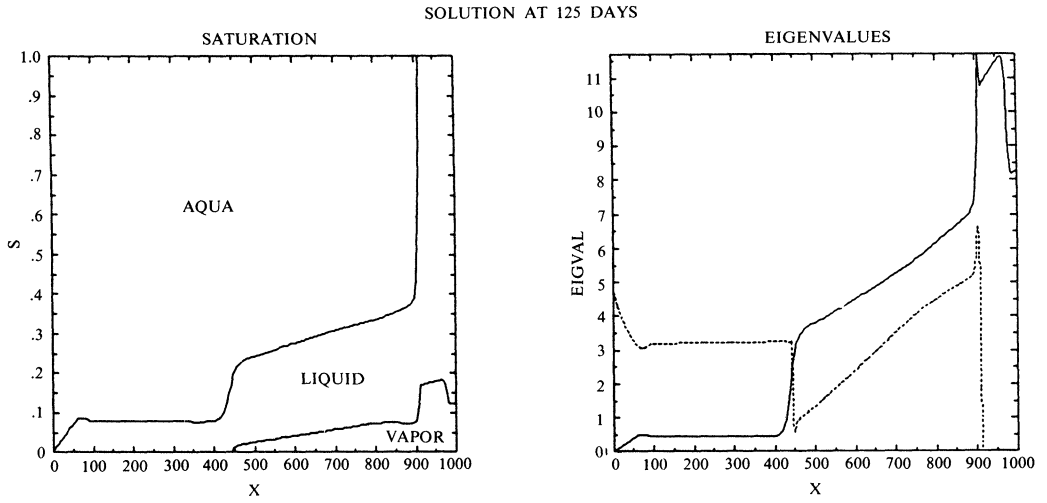

FIG. 7(b). *Saturations and wave speeds for second mixed flow example at late time.*

solutions typical of the Buckley–Leverett equation. When the fluid was undersaturated we retained one Buckley–Leverett wave; however, the other family, corresponding to a particle velocity eigenvalue, was linearly degenerate and produced only contact discontinuities.

We also demonstrated that additional effects caused by pressure changes or compositional variation could lead to problems in which several regimes were present and to an associated increase in complexity of the solution behavior. The computational results suggest that although the splitting was proposed primarily as a numerical device, the associated structure, in fact, provides at least a partial characterization of the analytic structure of the equations.

The analysis of this paper was a fully general analysis of the black-oil model. We analyzed the most general mass transfer and compressibility effects. Simpler cases, involving more restricted mass transfer or fewer than three components, can be treated by setting the appropriate parameters in our analysis to zero.

Finally, we emphasize that the motivation for this work was to establish the necessary analytic foundations for the design of high-resolution numerical methods for black-oil reservoir simulation. In particular, the characteristic structure of the component conservation equation discussed in § 6 provides the information needed to construct a second-order Godunov method for the system. The development of this type of numerical method as well as computational results for problems in one and two space dimension are discussed in Bell, Colella, and Trangenstein [5].

Appendix A. Units and functional forms. The spatial coordinate x has units of feet, and time t is measured in days. Pressure p is measured in psi, viscosity is measured in centipoise, and total permeability κ is measured in ft^2 cp/psi days, or .006328 times the value in millidarcies. For the computations in this paper, the reservoir had permeability $\kappa = 100md$, and porosity $\phi = 0.2 + 0.2 \times 10^{-5} p$.

For simplicity, we have chosen the relative permeability functions to be

$$\kappa_l = (1 - s_v - s_a)(1 - s_v)(1 - s_a),$$
$$\kappa_v = s_v^2, \qquad \kappa_a = s_a^2.$$

The liquid phase relative permeability is the result of using the standard square saturation relative permeability functions in conjunction with Stone's model.

The component densities n are measured in cubic feet at some reference condition (temperature and pressure) per reservoir cubic foot. Here we intend the mass of the component to be measured in terms of the volume it occupies under surface conditions, which are presumed to be at a different pressure and temperature than in the reservoir. As a result, the formation volume factors have the units of cubic feet per standard cubic foot.

We have chosen the following functional forms for the ratios:

$$R_l(p) = .05p,$$
$$R_v(p) = 9 \times 10^{-5} - 6 \times 10^{-8} p + 1.6 \times 10^{-11} p^2,$$
$$R_a(p) = .005p.$$

Individual black-oil models may choose to replace any or all of these functions by zero. Note that the condition $\det R = 1 - R_l R_v > 0$ is satisfied for all pressures above 0.

For the viscosities, we have chosen

$$\mu_l = \begin{cases} .8 - 1 \times 10^{-4} p & \text{if liquid is saturated,} \\ (.8 - 1 \times 10^{-4} p_b)(1 + 6.78 \times 10^{-5}(p - p_b)) & \text{if liquid is undersaturated,} \end{cases}$$

$$\mu_v = .012 + 3 \times 10^{-5} p,$$

$$\mu_a = \begin{cases} .35 & \text{if aqua is saturated,} \\ .35(1 + 6.78 \times 10^{-5}(p - p_b)) & \text{if aqua is undersaturated.} \end{cases}$$

The formation volume factors are the most complicated functions to describe:

$$B_l = \begin{cases} 1 - 2.31 \times 10^{-5} p & \text{if } R_l(p) \equiv 0, \\ 1 + 1.5 \times 10^{-4} p & \text{if liquid is saturated and } R_l > 0, \\ \dfrac{1 + 1.5 \times 10^{-4} p_b}{1 + 2.31 \times 10^{-5}(p - p_b)} & \text{if liquid is undersaturated,} \end{cases}$$

$$B_v = \begin{cases} \dfrac{1}{6 + .06p} & \text{if vapor is saturated,} \\ \dfrac{1}{7 + .06p} + \dfrac{\bar{R}_v}{R_v}\left[\dfrac{1}{6 + .06p} - \dfrac{1}{7 + .06p}\right] & \text{if vapor is undersaturated,} \end{cases}$$

$$B_a = \begin{cases} 1 - 1.8 \times 10^{-5} p & \text{if } R_a(p) \equiv 0, \\ 1 - 3 \times 10^{-6} p & \text{if aqua is saturated and } R_a > 0, \\ \dfrac{1 - 3 \times 10^{-6} p_b}{1 + 1.8 \times 10^{-5}(p - p_b)} & \text{if aqua is undersaturated.} \end{cases}$$

Note that neither R_l nor R_a have been taken to be identically zero in this paper. These extra cases in the definitions of B_l and B_a are provided for readers who wish to perform computations with alternative black-oil problems. For example, the standard black-oil model chooses $R_v \equiv 0$ and $R_a \equiv 0$.

Appendix B. Alternative formulation of the flux. In § 4.2 we mentioned an alternative definition of the component flux that gives an equally admissible sequential formulation of the component conservation equations. Instead of using equations (4.1)-(4.2), we could write the flux as $ND_s^{-1}\mathrm{v}$. In the saturated case, this gives us

$$h = RB^{-1}\mathrm{v}\, e^T u.$$

The characteristic analysis of the alternative component conservation equation gives us $(\partial h/\partial n)X = X\Lambda$, where

$$X \equiv RB^{-1}\begin{bmatrix} 1 & -e^T \\ 0 & I \end{bmatrix}\begin{bmatrix} 1 & 0 \\ 0 & X_C \end{bmatrix}\begin{bmatrix} 1 & 0 \\ -a & I \end{bmatrix},$$

$$\Lambda = \begin{bmatrix} \mathrm{v}_T & 0 \\ 0 & \Lambda_C \end{bmatrix}.$$

Here X_C is the same as in (6.1), but unlike (6.2) the vector a is determined by the following relations:

$$c \equiv [0 \quad I]v - C[0 \quad I]s, \qquad X_C(\Lambda_C a - a v_T) = c.$$

Only one of the left eigenvectors (i.e., rows of X^{-1}) is unchanged. It is the vector $e^T(\partial u/\partial n) = e^T BR^{-1}$, which shows that the total fluid volume is still a Riemann invariant. All of the eigenvalues are changed, although two are changed only by a factor of $e^T u$ (which should be close to one). The only eigenvalue that is changed significantly corresponds to the degenerate linear advection mode introduced by the splitting, which now moves with speed equal to the total fluid velocity.

For a three-component two-phase flow, the matrix of right eigenvectors for the alternative flux function is

$$X \equiv X_M \begin{bmatrix} X_{\bar{V}} & 0 \\ 0 & 1 \end{bmatrix} \begin{bmatrix} I & -a \\ 0 & 1 \end{bmatrix},$$

and the matrix of eigenvalues is

$$\Lambda = \begin{bmatrix} \Lambda_{\bar{V}}(1/e^T u) & 0 \\ 0 & \lambda \end{bmatrix}.$$

Here λ is the same as in (6.5), but

$$X_{\bar{V}}^{-1} \equiv \begin{bmatrix} 1 & 1 \\ s_a^2 \dfrac{\partial(v_a/s_a)}{\partial s_a} & s_*^2 \dfrac{\partial(v_*/s_*)}{\partial s_a} \end{bmatrix},$$

and

$$\Lambda_{\bar{V}} \equiv \begin{bmatrix} v_T & 0 \\ 0 & \partial v_a/\partial s_a \end{bmatrix}.$$

Also, we choose a as in (6.6) for the new values of $\Lambda_{\bar{V}}$ and $X_{\bar{V}}$. Only one of the left eigenvectors is unchanged from those in (6.7); it is proportional to the vector $\partial\omega/\partial n$, which shows that the undersaturation variable is still a Riemann invariant. Again, the most significant change in the eigenvalues is that the degenerate wave speed is changed from zero to v_T.

Acknowledgment. We would like to thank Jim Demmel for his kind help with linear algebra in the presence of eigenvector deficiencies.

REFERENCES

[1] G. Acs, S. Doleschall, and E. Farkas, *General purpose compositional model* (SPE 10515), in 6th SPE Symposium on Reservoir Simulation, New Orleans, LA, February 1982, pp. 385–404.

[2] K. Aziz and A. Settari, *Petroleum Reservoir Simulation*, Applied Science, 1979.

[3] J. B. Bell, G. R. Shubin, and J. A. Trangenstein, *A method for reducing numerical dispersion in two-phase black-oil reservoir simulation*, J. Comput. Phys., 65 (1986), pp. 71–106.

[4] J. B. Bell, J. A. Trangenstein, and G. R. Shubin, *Conservation laws of mixed type describing three-phase flow in porous media*, SIAM J. Appl. Math., 46 (1986), pp. 1000–1017.

[5] J. B. Bell, P. Colella, and J. A. Trangenstein, *Higher-order Godunov methods for general systems of hyperbolic conservations laws*, UCRL-97258, Lawrence Livermore National Laboratory, Livermore, CA, August 1987, J. Comput. Phys., to appear.

[6] P. Colella, *Multidimensional upwind methods for hyperbolic conservation laws*, LBL-17023, Lawrence Berkeley Laboratory, Berkeley, CA, July 1984, J. Comput. Phys., to appear.

[7] F. F. Craig, jr., *The reservoir engineering aspects of waterflooding*, Society of Petroleum Engineers of AIME, Dallas, 1971.

[8] E. L. Isaacson, *Global solution of the Riemann problem for a non-strictly hyperbolic system of conservation laws arising in enhanced oil recovery*, Department of Mathematical Physics, Rockerfeller University, New York.

[9] R. P. Kendall, G. O. Morrell, D. W. Peaceman, W. J. Silliman, and J. W. Watts, *Development of a multiple application reservoir simulator for use on a vector computer*, SPE Paper 11483, Manama, Bahrain, March, 1983.

[10] B. L. Keyfitz and H. C. Kranzer, *A system of non-strictly hyperbolic conservation laws arising in elasticity theory*, Arc. Rational Mech. Anal., 72 (1980), pp. 220–241.

[11] D. W. Peaceman, *Fundamentals of Numerical Reservoir Simulation*, Elsevier Scientific Publishing Company, New York, 1977.

[12] A. SPIVAK AND T. N. DIXON, *Simulation of Gas Condensate Reservoirs*, in 3rd Symposium on Numerical Simulation of Reservoir Performance, Houston, TX, 1973.

[13] J. W. WATTS, *A compositional formulation of the pressure and saturation equations* (SPE 12244), in 7th SPE Symposium on Reservoir Simulation, San Francisco, CA, November 1983, pp. 113–122.

[14] A. WEISER AND M. WHEELER, *On convergence of block-centered finite difference methods for elliptic problems*, SIAM J. Numer. Anal., 25 (1988), pp. 351–375.